Electrostatic Resonances of Corrugated Interfaces and Cylindrical Clusters

皺摺界面和柱形微粒群的靜電共振

CHOY, Chun Wing
蔡振榮

A Thesis Submitted in Partial Fulfillment
of the Requirements for the Degree of
Master of Philosophy
in
Physics

August 2007


香港中文大學
圖書館系統
02 SEP 2008
UNIVERSITY
LIBRARY SYSTEM
THE CHINESE UNIVERSITY OF HONG KONG

Thesis/Assessment Committee

Professor CHU, Ming Chung (Chair)
Professor YU, Kin Wah (Thesis Supervisor)
Professor WAN, Tsz Kai Jones (Committee Member)
Professor YAKUBO, Kousuke (External Examiner)

Abstract

The first part of the thesis is mainly concerned the development of the Green function formalism (GFF), which can be used to study the local field distribution near a periodic interface separating two homogeneous media of different dielectric constants. In GFF, the integral equations can be solved conveniently because of the existence of an analytic expression for the kernel (Greenian). However, due to a severe singularity in the Greenian, the formalism was formerly applied to compute the electric fields away from the interface region. In the thesis, we have been succeeded in extending GFF to compute the electric field inside the interface region by taking advantage of a sum rule. To our surprise, the strengths of the electric fields are quite similar in both media across the interface, despite of the large difference in the dielectric constants. Moreover, we propose a simple effective medium approximation (EMA) to compute the electric field inside the interface region. We show that EMA indeed give an excellent description of the electric field except near a surface plasmon resonance.

The second part of the thesis is concerned about Bergman-Milton electrostatic resonances. We have succeeded in applying GFF to compute the electrostatic resonance of cluster of two and three cylindrical particles. Numerical solutions of the eigenvalue equation yield a pole spectrum in the spectral representation and this pole spectrum is in turn used to compute the optical response of those particles. For two cylindrical particles, the results are in excellent agreement with the exact results from the multiple image method and

normal-mode expansion method. The results can be extended to investigate the enhanced nonlinear optical response of metal-dielectric composites, as well as optical switching in the plasmonic waveguides.

摘要

論文的第一個部分是關於格林函數方法(GFF)的發展。 它可以用於研究皺摺界面附近的局部電場分布。借助結構格林函數(Greenian)，我們可以輕易求出積分方程的解。但因結構格林函數的奇點，GFF只可計算遠離界面區的電場。我們在論文中成功利用求和定則延伸了GFF去計算界面區裡面的電場。雖然兩種物質的介電常數有很大的區別，但我們發現了橫跨兩種物質的電場是相當相似。而且，我們提出簡單的EMA估算在界面區裡面的電場。除在表面胞質共振的情況下，我們發現EMA能描述界面區裡面的電場。

論文的第二個部分是關於Bergman-Milton靜電共振。我們成功利用GFF計算二個和三個圓柱形微粒群的靜電共振。本徵值等式的解可以產生一個杆光譜，而這個杆光譜可以用於計算那些微粒的光學反應。我們的結果為完全符合二個圓柱形微粒真確的結果。而我們的結果可以引申去研究金屬電介質複合材料的非線性光學反應以及電漿波導管的光學開關。

Acknowledgments

I would like to take this opportunity to express my sincere gratitude to my supervisor Prof. Kin Wah Yu for his excellent guidance and advice. During my study, Prof. Yu had given me a lot of opportunities to explore the world like presenting in international physics conferences. I would also like to thank Dr. Jun Jun Xiao for his valuable advice and assistance on my research.

Special thanks are given to Miss Ying Wai Li, Mr Yue Hin Pong and Mr Kwan Yan Lee for their friendships and valuable memories in the two years.

Finally, I would like to thank my family as well as Miss Janette Wai Wun So for their unconditional support and encouragement.

Contents

List of Figures

List of Tables

Chapter 1

Introduction

1.1 Electric field near corrugated interfaces

Electric field distribution near corrugated interfaces have been investigated for a long time [1]. These corrugated interfaces occur in many important physical systems [2–5]. Theoretical calculations of the local field distribution requires a detailed solution of Maxwell's equation which is a difficult task for interfaces of complex geometry because of the complicated boundary conditions. So far, Yu *et al.* have established Green function formalism (GFF) to compute the local field distribution for an arbitrary interface separating two media of different dielectric constants without matching of complicated boundary conditions [6, 7]. They adopt similar treatment as Korringa, Kohn and Rostoker (KKR) method [8, 9] to introduce the structure Green's function (Greenian) to include the effect of periodicity by evaluating an infinite sum. Gu *et al.* applied introduce GFF in lattice systems [10–12]. Tam *et al.* [13] applied GFF to corrugated interfaces in two dimensions.

However, due to a severe singularity in the structure Green's function, the formalism was formerly applied to compute the electric fields away from the interface region. This is the main objective of the first part of the thesis, in which GFF had been extended to compute the electric field inside the interface region by taking advantage of a sum rule [14]. Surprisingly, we found that the

strength of electric field are quite similar in both media across the interface despite of the large difference in the dielectric constants. Moreover, we propose a simple effective medium approximation (EMA) to compute the electric field inside the interface region and we show that EMA gives an excellent description of the electric field except near a surface plasmon resonance. This provides a great insight that corrugated interfaces can be well described by graded interfaces, as suggested by the recent paper [15–17].

1.2 Electrostatic resonances of cylindrical clusters

Electrostatic resonances (ERs) is of great interest in engineering the electromagnetic properties of nanomaterials [18–20]. ERs are essentially source-free electrostatic fields appeared at specific negative dielectric permittivity [21, 22] that may find interesting applications in semiconductor nanoparticles because they can be controlled through optical manipulation of carrier densities. This optical controllability can be utilized for the development of nanoscale light switches and all-optical transistors. They also have significant implications in optical properties of composite nanomaterials and coupled surface plasmons in plasmonic structures [23–28], clearly reflected in the Bergman-Milton spectral representation [23–25, 29, 30]. Specifically, for composites consisting of two ingredients [e.g., $\epsilon_1(\omega)$ and $\epsilon_2(\omega)$], by using a spectral parameter $s(\omega) = [1 - \epsilon_1(\omega)/\epsilon_2(\omega)]^{-1}$, the material-independent eigenmodes $\{s_n, \phi_n(\mathbf{r})\}$ of ER are essentially determined by microstructure of the system [15, 23–25, 31]. Once the electrostatic resonant eigenvalues s_n and their residues f_n are established, the resonant frequencies are determined by the dielectric dispersion function $\epsilon_1(\omega)$ and the macroscopic effective optical properties, e.g.,

bulk dielectric permittivity ϵ_{eff}, of the system become readily known [23–26, 29, 30]. This theory has been extensively and successfully exploited for studies of optical random composites (for example, see Ref. [26]), graded composites [15], periodic nanostructures [18], as well as media of various geometries [19, 21, 22, 31]. It also facilitates studies of electrorheological fluid and electrokinetics of biological cells [32–34]. The formalism partially changes, however, when there are more than two constituent components, for example, in three-component composites discussed by Gu and Gong [35], and in graded composites as detailed by Dong *et al.* [36].

Regarding the influence of microstructures on the spectral functions s_n and f_n, a well known result is that s_n possesses discrete pole(s) for regular geometry inclusions whose sizes are much smaller than the wavelength concerned, for instance, $s = 1/2$ for individual cylinders [37, 38] and $s = 1/3$ [39] for individual spheres. However, when two such inclusions approach and form a dimer, due to the mutual electromagnetic interactions, the poles s_n become infinite series that asymptotically collapse at 1/3 and 1/2 for spherical and cylindrical non-touching dimers, respectively. The dimer case is an idea prototype in studying particle-particle interactions and has received much attention [38, 40–44]. Subsequently, one would request situations with increasing number of nanoparticles and complex geometry. This is the main objective of the second part of the thesis. By applying GFF, the pole spectra can be easily found regardless of the complex geometry. It turns out that the spectral poles become more complicated for complex geometry, but to calculate them is relatively easy under our scheme, in contrast to many traditional methods [17, 38, 41–45].

1.3 Objective of the thesis

In chapter 2, GFF by Yu *et al.* [6, 7] will be reiterated to establish notations. Some numerical results will also be presented to give a first glance of surface plasmon resonance.

In chapter 3, GFF is extended to compute the electric field inside the interface region by taking advantage of a sum rule [14]. We found that the strength of electric field are quite similar in both media across the interface despite of the large difference in the dielectric constants. Moreover, we propose a simple effective medium approximation (EMA) to compute the electric field inside the interface region and we show that EMA gives an excellent description of the electric field except near a surface plasmon resonance.

In chapter 4, we firstly derive the spectral representation formalism from GFF, which differs from traditional methods [17, 38, 41–45], is suitable for an arbitrary interface separating two media of different dielectric constants without matching of complicated boundary conditions. We then use it to numerically examine spectral functions of a pair of nanocylinders, which show results in good agreement with exact data from both multiple image method [45] and normal-mode expansion method [38]. Finally, we go further to extract the spectral functions of nanocylinders in a triangle which enables the investigation of particle-particle interaction as well as particle-pair interaction. Our results also in good agreement from multipole method [41]. The three-cylinder-in-triangle case represents a guideline for investigation on various cylinder arrays [46] which is also tractable by the GFF we developed. Finally, we present a brief summary in chapter 5.

Chapter 2

Review on Green Function Formalism

Green function formalism (GFF) computes the local field distribution for an arbitrary interface separating two media of different dielectric constants [6, 7]. By using the divergence theorem, the volume integral equation is converted into a surface integral equation and thus it greatly simplifies numerical solutions and yields accurate results for interfaces of arbitrary shape. Here we reiterate the formalism to establish notations.

2.1 Integral equation formalism

Consider an arbitrary interface S separating two media of different dielectric constants ϵ_1 and ϵ_2. The electrostatic potential $\phi(\mathbf{r})$ satisfies the following Laplace's equation:

$$\nabla \cdot [\epsilon(\mathbf{r}) \nabla \phi(\mathbf{r})] = -4\pi\rho(\mathbf{r}), \tag{2.1}$$

with standard boundary conditions on the interface, where $\rho(\mathbf{r})$ is the free charge density, $\epsilon(\mathbf{r})$ equals ϵ_1 in the embedding medium and ϵ_2 in the host.

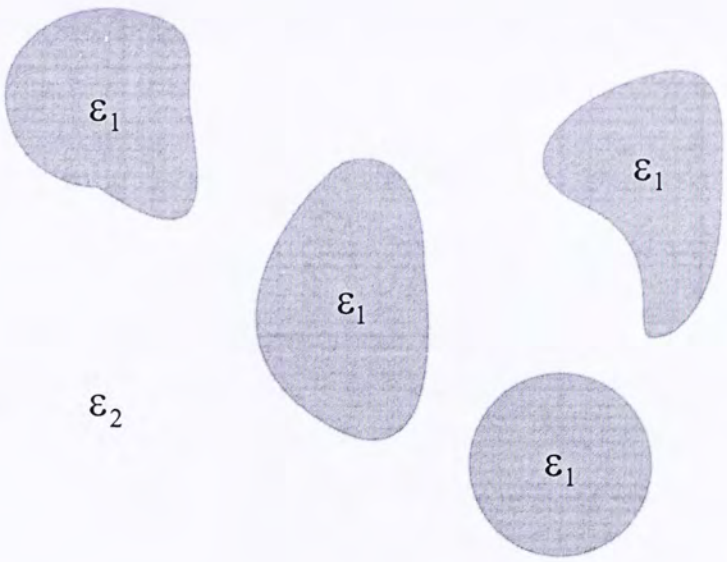

Figure 2.1: Schematic diagram showing material with dielectric constant ϵ_1 embedding in homogeneous medium with dielectric constant ϵ_2.

Let V_1 and V_2 be the volume of the embedding and the host medium, separating by an arbitrary interface S. Denoting $\theta(\mathbf{r}) = 1$ if $\mathbf{r} \in V_1$ and 0 otherwise, gives

$$\epsilon(\mathbf{r}) = \epsilon_2[1 - u\theta(\mathbf{r})], \tag{2.2}$$

where

$$u = 1 - \frac{\epsilon_1}{\epsilon_2}. \tag{2.3}$$

Putting equation (2.2) into equation (2.1), we have

$$\nabla^2\phi(\mathbf{r}) = -\frac{4\pi\rho(\mathbf{r})}{\epsilon_2} + u\nabla \cdot [\theta(\mathbf{r})\nabla\phi(\mathbf{r})]. \tag{2.4}$$

Let $G(\mathbf{r}, \mathbf{r}') = 1/|\mathbf{r} - \mathbf{r}'|$ and equation (2.4) admits a formal solution

$$\phi(\mathbf{r}) = -\frac{1}{4\pi}\int d\mathbf{r}' G(\mathbf{r}, \mathbf{r}')\left\{\frac{-4\pi\rho(\mathbf{r}')}{\epsilon_2} + u\nabla' \cdot [\theta(\mathbf{r}')\nabla'\phi(\mathbf{r}')]\right\}. \tag{2.5}$$

Equation (2.5) can be easily simplified to

$$\phi(\mathbf{r}) = \phi_0(\mathbf{r}) - \frac{u}{4\pi}\int d\mathbf{r}' G(\mathbf{r}, \mathbf{r}')\nabla' \cdot [\theta(\mathbf{r}')\nabla'\phi(\mathbf{r}')], \tag{2.6}$$

where $\phi_0(\mathbf{r}) = \frac{1}{\epsilon_2}\int dr' G(\mathbf{r},\mathbf{r}')\rho(\mathbf{r}')$ which is the solution of $\nabla^2\phi_0 = -4\pi\rho/\epsilon_2$. Consider the identity $f\nabla'\cdot\mathbf{A} = \nabla'\cdot(f\mathbf{A}) - (\nabla' f)\cdot\mathbf{A}$, where $f = G(\mathbf{r},\mathbf{r}')$ and $\mathbf{A} = \theta(\mathbf{r}')\nabla'\phi(\mathbf{r}')$, the volume integral in equation (2.6) can be separated into two integrals. The first integral is zero by divergence theorem and so we have

$$\phi(\mathbf{r}) = \phi_0(\mathbf{r}) + \frac{u}{4\pi}\int_{V_1} d\mathbf{r}'\nabla' G(\mathbf{r},\mathbf{r}')\cdot\nabla'\phi(\mathbf{r}'). \tag{2.7}$$

Consider the identity $\mathbf{A}\cdot\nabla' f = \nabla'\cdot(f\mathbf{A}) - (\nabla'\cdot\mathbf{A})f$, where $f = \phi$ and $\mathbf{A} = \nabla' G(\mathbf{r},\mathbf{r}')$, the volume integral above can be separated into two integrals and can be written as

$$\int_{V_1} d\mathbf{r}'\nabla' G(\mathbf{r},\mathbf{r}')\cdot\nabla'\phi(\mathbf{r}') = \oint_S dS'[\hat{\mathbf{n}}'\cdot\nabla' G(\mathbf{r},\mathbf{r}')]\phi(\mathbf{r}') + 4\pi\theta(\mathbf{r})\phi(\mathbf{r}), \tag{2.8}$$

where $\hat{\mathbf{n}}'$ is the unit normal to S pointing from medium 1 to medium 2. As a result, we have

$$[1 - u\theta(\mathbf{r})]\phi(\mathbf{r}) = \phi_0(\mathbf{r}) + \frac{u}{4\pi}\oint_S dS'[\hat{\mathbf{n}}'\cdot\nabla' G(\mathbf{r},\mathbf{r}')]\phi(\mathbf{r}'). \tag{2.9}$$

We now aim to solve a surface integral equation for the potential at the expense of a two-step solution [7]:

1. step 1: determine $\phi(\mathbf{r})$ for all $\mathbf{r}\in S$ by solving equation (2.9), and then
2. step 2: obtain $\phi(\mathbf{r})$ for all $\mathbf{r}$ by using equation (2.9) and the results of step 1.

In step 1, we encounter a singularity when the integration variable $\mathbf{r}'$ approaches the point of observation $\mathbf{r}$. In order to tackle the problem, we take an infinitesimal volume around $\mathbf{r}$ and perform the surface integral equation analytically, we find [7]

$$\left(1 - \frac{u}{2}\right)\phi(\mathbf{r}) = \phi_0(\mathbf{r}) + \frac{u}{4\pi}\oint_S{}' dS'[\hat{\mathbf{n}}'\cdot\nabla' G(\mathbf{r},\mathbf{r}')]\phi(\mathbf{r}'), \mathbf{r}\in S, \tag{2.10}$$

where prime denotes a restricted integration which excludes $\mathbf{r}' = \mathbf{r}$. The surface integral equation (2.10) can be solved for $\phi(\mathbf{r}\in S)$.

2.2 Periodic corrugated interfaces

In this section, we apply the integral equation formalism to a periodic interface. Suppose the interface profile depends only on x, described by $y = f(x)$, where $f(x)$ is a periodic function of x with period $L : f(x+L) = f(x)$. Thus medium 1 occupies the space $y < f(x)$ while medium 2 occupies the space $y > f(x)$ separated by the interface at $y = f(x)$. The external field is $\mathbf{E}_0 = E_0\hat{\mathbf{y}}$ and $\phi_0 = -\mathbf{E}_0 \cdot \hat{\mathbf{r}}$. For a periodic system, $\phi(\mathbf{r})$ is a periodic function of the lattice vector $\mathbf{T} = mL\hat{\mathbf{x}}$, where m is an integer. In what follows, we adopt similar treatment as the Korringa, Kohn and Rostoker (KKR) method [8, 9] and rewrite the integral equation (2.10) as

$$\left(1 - \frac{u}{2}\right)\phi(\mathbf{r}) = -\mathbf{E}_0 \cdot \mathbf{r} + \frac{u}{4\pi}\int_{uc}' dS'\tilde{G}(\mathbf{r},\mathbf{r}')\phi(\mathbf{r}'), \tag{2.11}$$

where the integration is performed within a unit cell. Since the interface is one-dimensional, the integral equation (2.11) becomes

$$\left(1 - \frac{u}{2}\right)\phi(\mathbf{r}) = -\mathbf{E}_0 \cdot \mathbf{r} + \frac{u}{4\pi}\int_{S}' dl'\tilde{G}(\mathbf{r},\mathbf{r}')\phi(\mathbf{r}'), \tag{2.12}$$

where the structure Green's function (Greenian) is given by

$$\tilde{G}(\mathbf{r},\mathbf{r}') = \sum_{\mathbf{T}} \hat{\mathbf{n}}' \cdot \nabla' G(\mathbf{r},\mathbf{r}'+\mathbf{T}) = \sum_{m=-\infty}^{+\infty} \frac{2\hat{\mathbf{n}} \cdot (\mathbf{r}-\mathbf{r}'-mL\hat{\mathbf{x}})}{|\mathbf{r}-\mathbf{r}'-mL\hat{\mathbf{x}}|^2}. \tag{2.13}$$

In view of the complicated calculus, the evaluation of the Greenian is a formidable task. However, by invoking the complex function $z = x + iy$, $z' = x' + if(x')$, we are able to evaluate the Greenian analytically as follows:

$$\begin{aligned} \hat{\mathbf{n}}' &= i\frac{dz'/dx'}{|dz'/dx'|} = \frac{-f'(x')+i}{\sqrt{1+[f'(x')]^2}}, \\ \mathbf{r}-\mathbf{r}'-mL\hat{\mathbf{x}} &= z - z' - mL. \end{aligned} \tag{2.14}$$

The summation element can be written as:

$$\begin{aligned} \frac{2\hat{\mathbf{n}} \cdot (\mathbf{r}-\mathbf{r}'-mL\hat{\mathbf{x}})}{|\mathbf{r}-\mathbf{r}'-mL\hat{\mathbf{x}}|^2} &= \frac{2\mathrm{Re}\left\{i\frac{dz'/dx'}{|dz'/dx'|}(z-z'-mL)^*\right\}}{|z-z'-mL|^2} \\ &= 2\mathrm{Re}\left\{i\frac{dz'/dx'}{|dz'/dx'|}\frac{1}{z-z'-mL}\right\}, \end{aligned} \tag{2.15}$$

and the Greenian can be written as:

$$\tilde{G}(\mathbf{r},\mathbf{r}') = \mathrm{Re}\left\{ 2i \frac{dz'/dx'}{|dz'/dx'|} \sum_{m=-\infty}^{+\infty} \frac{1}{z - z' - mL} \right\}. \tag{2.16}$$

The infinite sum in (2.16) can be evaluated by using the identity [47]:

$$\sum_{m=-\infty}^{\infty} \frac{1}{z-m} = \pi \cot(\pi z). \tag{2.17}$$

Using the above identity, the infinite sum can be rewritten as follows:

$$\sum_{m=-\infty}^{\infty} \frac{1}{z - z' - mL} = \frac{\pi}{L} \frac{\sin \frac{2\pi}{L}(x-x') - i \sinh \frac{2\pi}{L}(y - f(x'))}{\cosh \frac{2\pi}{L}(x-x') - \cos \frac{2\pi}{L}(y - f(x'))}. \tag{2.18}$$

Putting equations (2.14), (2.16) and (2.18) together, we get

$$\tilde{G}(\mathbf{r},\mathbf{r}') = \frac{2\pi}{L} \frac{f'(x') \sin \frac{2\pi}{L}(x-x') - \sinh \frac{2\pi}{L}(y - f(x'))}{\sqrt{1 + [f'(x')]^2}[\cos \frac{2\pi}{L}(x-x') - \cosh \frac{2\pi}{L}(y - f(x'))]}. \tag{2.19}$$

We would like point out that equation (2.19) is a truly remarkable result in which the analytic expression is valid for any arbitrary interface profile. If we consider a planar interface, $f(x) = f'(x) = 0$, then $\tilde{G} = 0$ and $\phi = 0$ on the interface, as expected. If the point of observation (x, y) is located at the interface, the Greenian has a finite limit as $x \to x'$:

$$\tilde{G}(x, f(x); x', f(x') | x' \to x) = \frac{f''(x)}{\{1 + [f'(x)]^2\}^{3/2}}. \tag{2.20}$$

Now, we can solve equation (2.12) for the potential $\phi(x, f(x))$ right at the interface. Since $dl' = \sqrt{1 + [f'(x')]^2} dx'$, equation (2.12) becomes

$$\left(1 - \frac{u}{2}\right) \phi(x, f(x)) = -E_0 f(x) + \frac{u}{4\pi} \int dx' \tilde{G}_{\mathrm{line}}(x, f(x); x', f(x')) \phi(x', f(x')), \tag{2.21}$$

where

$$\tilde{G}_{\mathrm{line}}(x, y; x', f(x')) = \frac{2\pi}{L} \frac{f'(x') \sin \frac{2\pi}{L}(x-x') - \sinh \frac{2\pi}{L}(y - f(x'))}{\cos \frac{2\pi}{L}(x-x') - \cosh \frac{2\pi}{L}(y - f(x'))}. \tag{2.22}$$

and

$$\tilde{G}_{\mathrm{line}}(x, f(x); x', f(x') | x' \to x) = \frac{f''(x)}{1 + (f'(x))^2} \tag{2.23}$$

The subscript 'line' is put to remind us that this Greenian is used when doing integration along the line $y = 0$.

Then, we can use equation (2.22) to find the potential at any arbitrary point $(x, y) \notin S$, using the potential at the interface.

$$[1 - u\theta(f(x) - y)]\,\phi(x, y) = -E_0 y + \frac{u}{4\pi}\int dx' \tilde{G}_{\text{line}}(x, y; x', f(x'))\phi(x', f(x')), \tag{2.24}$$

where $\theta(x) = 0$ for $x < 0$, and $\theta(x) = 1$ for $x > 0$. The electric field is computed by the negative gradient of the potential. We find the electric field at the interface and in medium 1 and 2:

$$E_{1x} = -\frac{1}{1-u}\left(\frac{u}{4\pi}\int dx' \frac{\partial \tilde{G}_{\text{line}}}{\partial x}\phi(x', f(x'))\right), \tag{2.25}$$

$$E_{1y} = \frac{1}{1-u}\left(E_0 - \frac{u}{4\pi}\int dx' \frac{\partial \tilde{G}_{\text{line}}}{\partial y}\phi(x', f(x'))\right), \tag{2.26}$$

$$E_{2x} = -\frac{u}{4\pi}\int dx' \frac{\partial \tilde{G}_{\text{line}}}{\partial x}\phi(x', f(x')), \tag{2.27}$$

$$E_{2y} = E_0 - \frac{u}{4\pi}\int dx' \frac{\partial \tilde{G}_{\text{line}}}{\partial y}\phi(x', f(x')), \tag{2.28}$$

$$E_{\text{in},x} = -\frac{1}{1-u/2}\left(\frac{u}{4\pi}\int dx' \frac{\partial \tilde{G}_{\text{line}}}{\partial x}\Big|_{y=f(x)}\phi(x', f(x'))\right), \tag{2.29}$$

$$E_{\text{in},y} = -\frac{1}{1-u/2}\left(E_0 - \frac{u}{4\pi}\int dx' \frac{\partial \tilde{G}_{\text{line}}}{\partial y}\Big|_{y=f(x)}\phi(x', f(x'))\right). \tag{2.30}$$

The partial derivatives of the Greenian can be computed analytically from equation (2.22)

$$\frac{\partial \tilde{G}_{\text{line}}(x, y; x', f(x'))}{\partial x} = -\frac{4\pi^2}{L^2}\frac{f'(x')\,(\cos a \cosh b - 1) + \sin a \sinh b}{(\cos a - \cosh b)^2},$$

$$\frac{\partial \tilde{G}_{\text{line}}(x, y; x', f(x'))}{\partial y} = \frac{4\pi^2}{L^2}\frac{f'(x')\sin a \sinh b - \cos a \cosh b + 1}{(\cos a - \cosh b)^2},$$

where

$$\begin{aligned} a &= \frac{2\pi}{L}(x - x'), \\ b &= \frac{2\pi}{L}(y - f(x')). \end{aligned}$$

2.3 Solution by mode expansion

To solve the integral equation, we express the potential at an arbitrary point into a mode expansion:

$$\phi(x, y) = \sum_{jk} C_{jk}\psi_j(x)\xi_k(y - f(x)), \tag{2.31}$$

where $\psi_j(x)$ and $\xi_k(y)$ are mode functions. The potential on the interface can be expressed as:

$$\phi(x, f(x)) = \sum_{jk} C_{jk}\psi_j(x)\xi_k(0) = \sum_j A_j\psi_j(x), \tag{2.32}$$

where $A_j = \sum_k C_{jk}\xi_k(0)$. Substituting the mode expansion equation (2.32) into equation (2.21) and integrating whole equation by the factor $\int dx\psi_i(x)$, the coefficients A_j satisfy the matrix equation:

$$\left[\left(1 - \frac{u}{2}\right)\mathbf{B} - \frac{u}{4\pi}\mathbf{M}\right]\mathbf{A} = -E_0\mathbf{V}, \tag{2.33}$$

where

$$B_{ij} = \int dx\psi_i(x)\psi_j(x), \tag{2.34}$$

$$M_{ij} = \int\int dxdx'\psi_i(x)\tilde{G}_{\text{line}}(x, f(x); x', f(x'))\psi_j(x'), \tag{2.35}$$

$$V_i = \int dx\psi_i(x)f(x). \tag{2.36}$$

Here we would like to discuss the choice of modes function. The choice of the mode function is actually arbitrary in theory. However, the mode functions should be simple to use in practice. Common choice of mode functions are

step functions, triangular function and Fourier series expansion. The choices of different mode functions had been investigated in ref. [13]. It should be noted that the matrix **B** should be diagonal when we choose step functions as our mode function.

The evaluation of **M** involves the Greenian which is singular when $x = x'$. Hence, limit (2.23) should be used if $i = j$ for M_{ij}. After we compute the matrices **B**, **V** and **M**, A_j can be determined and the potential at the interface can be obtained by eq. (2.32). Then the potential at all spaces can be found by equation (2.24) and the electric field can be found by equations (2.25) to (2.28).

2.4 Numerical Results

In this section, we would like review some numerical results by Formalism. The following interface was adopt from numerical calculation.

$$f(x) = -\cos\frac{2\pi x}{L} - 0.1\sin\frac{4\pi x}{L} \tag{2.37}$$

where L and E_0 are set to be 1 without loss of generality. The interface profile is shown in figure 2.2. In what follows, we adopt 100 step functions as the mode functions, equally spaced in the unit interval $x \in (-0.5, 0.5]$. Moreover, ϵ_2 is chosen to be 1. The interface profile is shown in figure 2.2.

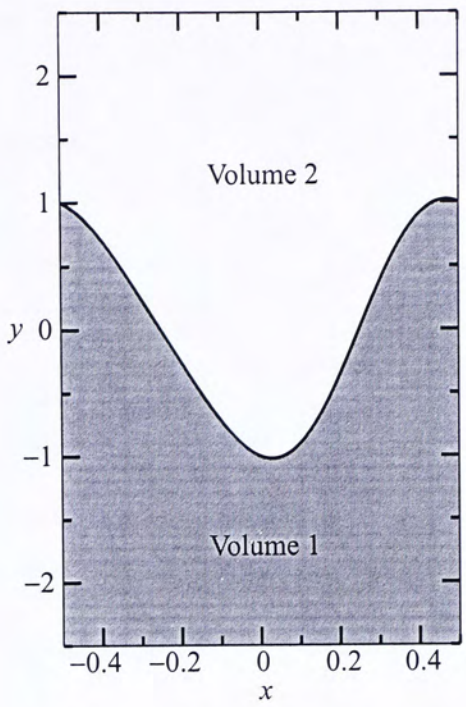

Figure 2.2: The interface profile $y = -\cos 2\pi x - 0.1 \sin 4\pi x$ plotted against x. Volume 1 is shaded in red colour.

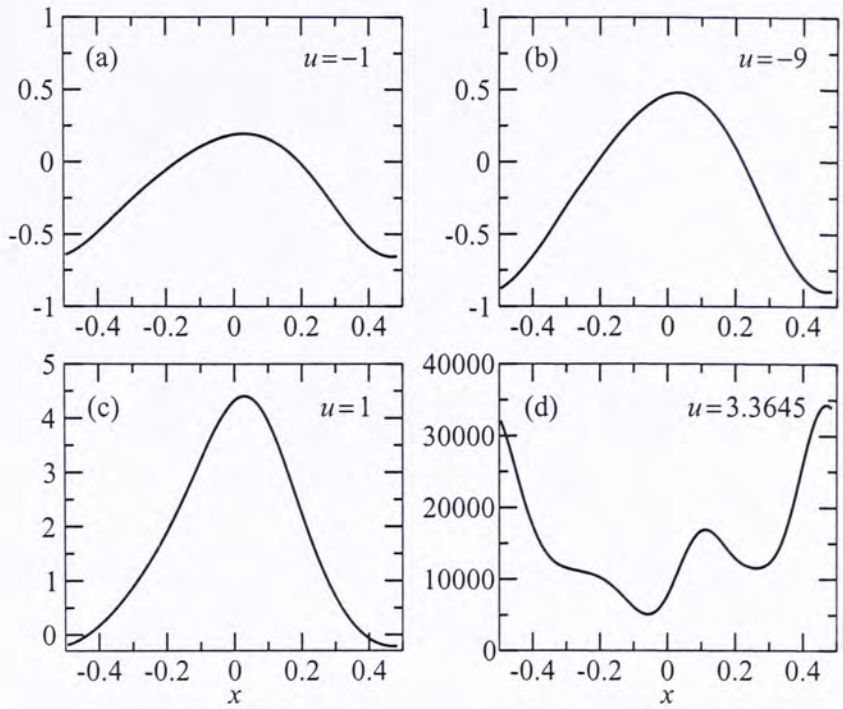

Figure 2.3: The electric potential ϕ at the interface for different u. (a) $u = -3$; (b) $u = -1$; (c) $u = 1$; (d) $u = 3.3645$. Note the great enhancement of ϕ in (d) corresponds to surface plasmon resonance.

We have calculated the electric potential ϕ right at the interface by using different parameters of u. The results are shown in figure 2.3. For negative values of u, it can be seen that the variation of potential increases when the dielectric contrast increases. It is interesting to the giant enhancement of the electric potential, as shown in figure 2.3 (d). The enhancement of the electric potential corresponds to the surface plasmon resonance, which is the nontrivial solution of equation (2.33) in the absence of external electric field [13]. In fact, the resonance state only occur at some particular values of u (or ϵ_1/ϵ_2) and these are the poles in Bergman-Milton spectral representation. More discussion on these poles will be provided in chapter 4.

Chapter 3

Electric Field at the Interface

In the previous chapter, GFF have been reviewed. Since there is a severe singularity in the partial derivative of the Greenian, it is not possible to calculate the electric field right at the interface and the formalism was formerly applied to compute the electric fields away from the interface region [7]. As shown in this chapter, we would tackle this singularity by means of a sum rule [14]. To our surprise, the strengths of the electric fields are quite similar in both media across the interface, despite of the large difference in dielectric constant. Moreover, we propose a simple effective medium approximation (EMA) to compute the electric field inside the interface region. We show that EMA can indeed give an excellent description of the electric field, except near a surface plasmon resonance. This provides a great insight that corrugated interfaces can be well described by graded interfaces, as suggested in recent paper [14–17].

3.1 Formalism

When we try to evaluate the electric potential and electric field at the interface using equations 2.29 and 2.30, singularity of Greenian and its partial derivatives are involved. For the calculation of electric potential, the evaluation of $\mathbf{M}$ involves the Greenian which is singular when $x' \to x$. As a result, limit (2.23) should be used for $i = j$ for M_{ij}. For the calculation of electric field

at the interface, the partial derivatives of the Greenian diverge when $x' \to x$ and they do not possess finite limit as in equation (2.23). Fortunately, we can tackle this severe singularity by means of a sum rule. For the application of the sum rule, we should restrict the mode function to localized functions [13]. In particular, we choose step function as our mode functions:

$$\psi_i(x) = \begin{cases} 1 & , x_i - \frac{h}{2} < x < x_i + \frac{h}{2}; \\ 0 & , \text{otherwise} \end{cases} \tag{3.1}$$

where h is the width of the step functions. Substituting the mode expansion (2.32) into equations (2.29) and (2.30) and integrating both sides by the factor $\int dx\psi_i(x)$, the following matrix equations can be obtained:

$$\mathbf{E}_x = -\frac{1}{1-u/2}\left(\frac{u}{4\pi}\right)\mathbf{K}_x \cdot \mathbf{A}, \tag{3.2}$$

$$\mathbf{E}_y = \frac{1}{1-u/2}\left(\mathbf{E}_0 - \frac{u}{4\pi}\right)\mathbf{K}_y \cdot \mathbf{A}, \tag{3.3}$$

where

$$E_{x,i} = \int dx\psi_i(x)E_x(x, f(x)), \tag{3.4}$$

$$E_{y,i} = \int dx\psi_i(x)E_y(x, f(x)), \tag{3.5}$$

$$E_{0,i} = \int dx\psi_i(x)E_0, \tag{3.6}$$

$$K_{x,ij} = \int dx \int dx'\psi_i(x)\psi_j(x') \left.\frac{\partial \tilde{G}}{\partial x}\right|_{y=f(x)}, \tag{3.7}$$

$$K_{y,ij} = \int dx \int dx'\psi_i(x)\psi_j(x') \left.\frac{\partial \tilde{G}}{\partial y}\right|_{y=f(x)}, \tag{3.8}$$

and $\mathbf{A}$ is the matrix as encountered in (2.33). The electric field at the interfaces can be obtained by evaluating $\mathbf{E}_x$ and $\mathbf{E}_y$ in equations (3.4) and (3.5). However, the singularity of partial derivatives of Greeenian prevent us from evaluating the diagonal element of $\mathbf{K}_x$ and $\mathbf{K}_y$. Fortunately, the matrices $\mathbf{K}_x$ and $\mathbf{K}_y$

possess sum rules:

$$\sum_j K_{x,ij} = 0, \tag{3.9}$$

$$\sum_j K_{y,ij} = 0. \tag{3.10}$$

The problem is solved with the use of sum rules (3.9) and (3.10). Now, the off diagonal elements of $\mathbf{K}_x$ and $\mathbf{K}_y$ can be computed by using equations (3.7) and (3.8) for $i \neq j$ while the diagonal elements can be obtained by using following equations:

$$K_{x,ii} = -\sum_{j \neq i} K_{x,ij}, \tag{3.11}$$

$$K_{y,ii} = -\sum_{j \neq i} K_{y,ij}. \tag{3.12}$$

In this way, we can get all the elements of $\mathbf{K}_x$ and $\mathbf{K}_y$. The electric fields at the interfaces can then be obtained by computing (3.2) and (3.3). Here we would like to prove the above sum rules. We first write out the left hand side of (3.9) explicitly,

$$\begin{aligned}\sum_{j=1}^{n} K_{x,ij} &= \sum_{j=1}^{n} \int dx \psi_i(x) \int dx' \frac{\partial \tilde{G}_{\text{line}}(x, y; x', f(x'))}{\partial x} \Big|_{y=f(x)} \psi_j(x') \\ &= \int dx \psi_i(x) \int dx' \frac{\partial \tilde{G}_{\text{line}}(x, y; x', f(x'))}{\partial x} \Big|_{y=f(x)} \sum_{j=1}^{n} \psi_j(x').\end{aligned}$$

Since we have chosen step function as our mode function, it satisfies

$$\sum_{j=1}^{n} \psi_j(x') = 1. \tag{3.13}$$

Putting equation (3.13) into the above equation, we have

$$\sum_{j=1}^{n} K_{x,ij} = \int dx \psi_i(x) \frac{\partial}{\partial x} \left[\int dx' \tilde{G}_{\text{line}}(x, y; x', f(x')) \right]_{y=f(x)}. \tag{3.14}$$

Equation (3.14) can be transformed to

$$\sum_{j=1}^{n} K_{x,ij} = \int dx \psi_i(x) \frac{\partial}{\partial x} \left[\oint_s' dS' [\hat{\mathbf{n}} \cdot \nabla' G(\mathbf{r}, \mathbf{r}')] \right]_{y=f(x)} . \tag{3.15}$$

The factor $-\nabla' G(\mathbf{r}, \mathbf{r}')$ is just the electric field of a point charge at $\mathbf{r}$. Since $\mathbf{r}$ does not stay inside the region bounded by interface S, by Gauss law, the surface integral is zero. Hence, equation (3.9) is proved. Equation (3.10) can be proved in a similar way.

3.2 Numerical Results

To illustrate numerical results, we adopt the interface profile (2.37) for numerical computation. 100 steps function are used as mode functions. We have attempted the following calculations:

1. We compute the electric field at the interface for $u = -3$ (positive ϵ_1/ϵ_2 ratio) and $u = 3.3645$ (surface plasmon resonance).

2. We also compute the E_y at different y plates (*inside* and *outside* the interface region). As an illustration, we choose $y = 0$, 0.3, 1.1 and 2. For $y = 1.1$ and 2, all the points lie inside medium 2. For $y = 0$ or 0.3, some points lie inside medium 1 and some lie inside medium 2. Figure 3.1 gives a pictorial description.

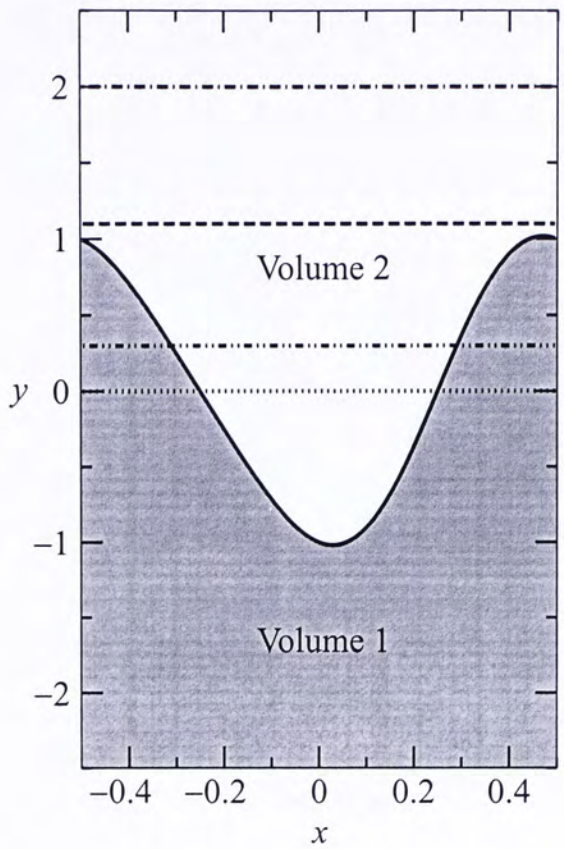

Figure 3.1: The interface profile $y = -\cos 2\pi x - 0.1 \sin 4\pi x$ (solid line) and $y = 0$, 0.3, 1.1 and 2 (dotted lines) plotted against x. It is clear that the lines $y = 0$ and 0.3 lie *inside* the interface region while the lines $y = 1.1$ and 2 lie *outside* the interface region.

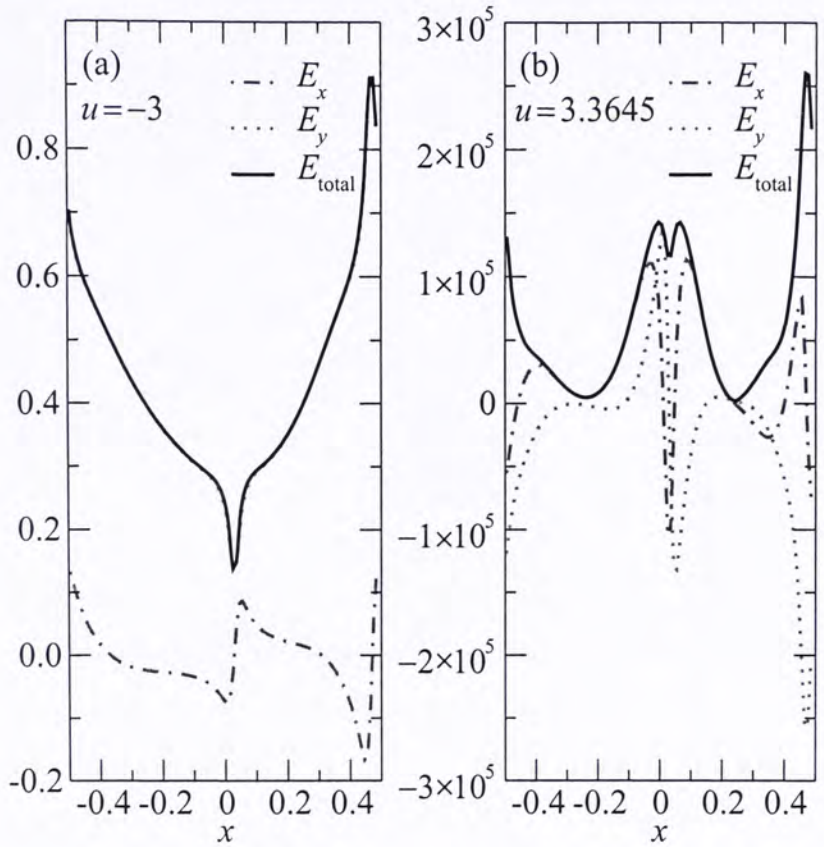

Figure 3.2: E_x(dash-dotted), E_y(dotted) and E_{total}(solid) at the interface plotted against x for $u = -3$ and 3.3645. It can be seen that the electric field changes gradually even in the case of surface plasmon resonance.

Without loss of generality, we choose $E_0 = 1$. Figure 3.2 (a) and (b) give the results for the electric field (E_x, E_y and $E_{\text{total}} = \sqrt{E_x^2 + E_y^2}$) at the interface for $u = -3$ and $u = 3.3645$ respectively. It can be seen that the electric field on the interface changes gradually in both cases. Comparing figure 3.2 (a) and (b), it is clear that the electric field enhances greatly in figure 3.2 (b). The reason behind this enhancement is surface plasmon resonance.

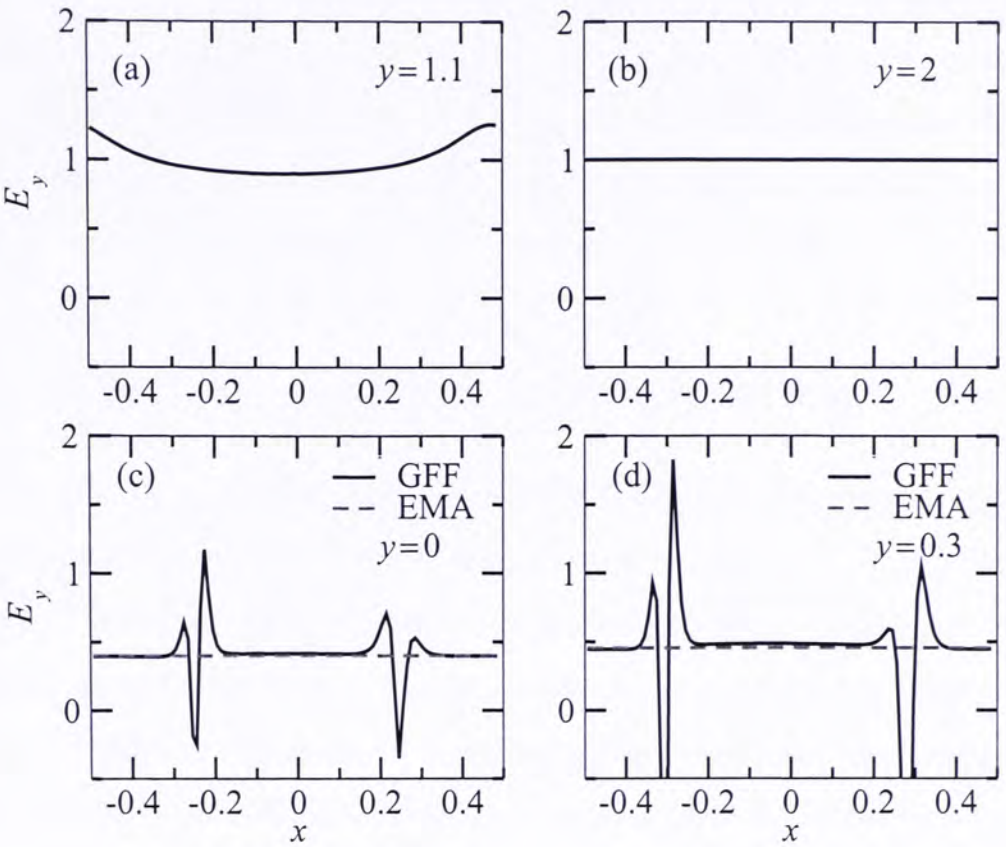

Figure 3.3: E_y found by GFF (solid line) and E_y found by EMA (dots) plotted against x for $u = -3$ at different y-slices. (a) $y = 1.1$; (b) $y = 2$; (c) $y = 0$; (d) $y = 0.3$.

It is also interesting to calculate E_y at different horizontal plates. Figure 3.3 shows the results E_y at different horizontal plates for $u = -3$. In figure 3.3 (a), it is found that $E_y(y = 1.1)$ exhibits variation because of the influence of bound charges at the interface. As a whole, $E_y(y = 1.1)$ has an average value of 1. On the other hand, $E_y(y = 2)$ is nearly a constant of 1 as shown in figure 3.3 (b). The electric field in this case equals the external electric field. This shows that the effect of the interface is negligible at large distance.

Figure 3.3(c) and (d) show the results for $y = 0$ and 0.3 respectively. In these two cases, E_y are quite similar inside both medium 1 and medium 2,

except for the points near the interface. This finding is surprising. Since $\epsilon_1 = 4\epsilon_2$, one should predict that $E_{1y} \approx 0.25E_{2y}$. We have also calculated E_y at other horizontal plates and E_{1y} and E_{2y} are also found to be quite similar. It is interesting to note that E_{1y} and E_{2y} are quite similar despite they have different representations as given by equations 2.26 and 2.28.

3.3 Effective medium approximation

Effective medium approximation (EMA), which was introduced by Bruggeman in 1935, is another approach to approximate electric field [23]. It is a mean-field theory and has a virtue of relative mathematical simplicity and of conceptual simplicity as well. However, it is a crude method and only gives approximate field. It is instructive to estimate E_y by using simple effective medium approximation (EMA). The effective dielectric constant ϵ can be found by weighted average of ϵ_1 and ϵ_2:

$$\epsilon = p_1\epsilon_1 + (1 - p_1)\epsilon_2, \tag{3.16}$$

where p_1 is the volume fraction of medium 1. In the fixed y plate, p_1 can be regarded as the length of line segment in medium 1 with a unit cell (For $L = 1$). With the effective dielectric constant ϵ, E_y can then be obtained easily through

$$E_y = \frac{E_0}{\epsilon}. \tag{3.17}$$

Figure 3.4(b) shows the effective dielectric constant with respect to y for $u = -3$, which means that ϵ_1 equals 4 and ϵ_2 equals 1. The interface profile is shown in figure 3.4 (a) for reference. It can be seen that the effective dielectric constant changes gradually across the interface, from 1 to 4.

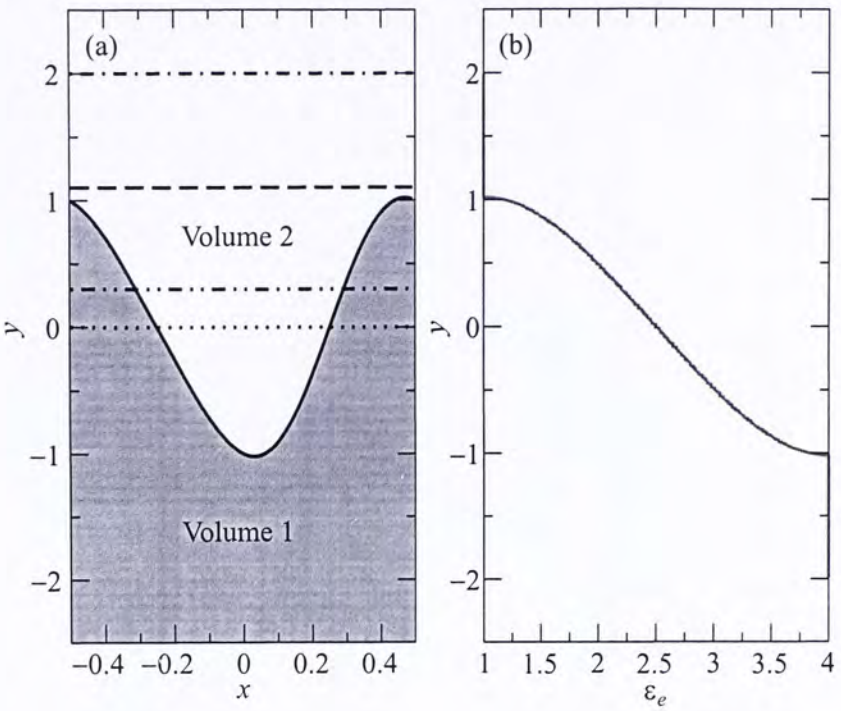

Figure 3.4: (a) The interface profile $y = -\cos 2\pi x - 0.1 \sin 4\pi x$ (solid line) and $y = 0$, 0.3, 1.1 and 2 (dotted lines) plotted against x. (b) The effective dielectric constant with respect to y. It can be seen that the effective dielectric constant changes gradually across the corrugated interface.

Figure 3.3 (c) and (d) shows the results with EMA. It is clear that the electric field predicted by simple effective medium approximation matches the electric field calculated by GFF for $u = -3$. In general, simple EMA gives excellent description of E_y for negative u in which surface plasmon resonance is absent. In fact, EMA is just a crude method to estimate electric field in heterogeneous media. It is surprising that this crude method gives excellent description of the electric fields for negative ϵ_1/ϵ_2 ratio. We also calculated E_y at $y = 0$ for $u = 3.3645$ (surface plasmon resonance), as shown in figure 3.5. Obviously, the electric field has a great enhancement this time. Simple EMA fails to predict this enhancement. Here we would like to emphasize that electric field can still be found by GFF in this case.

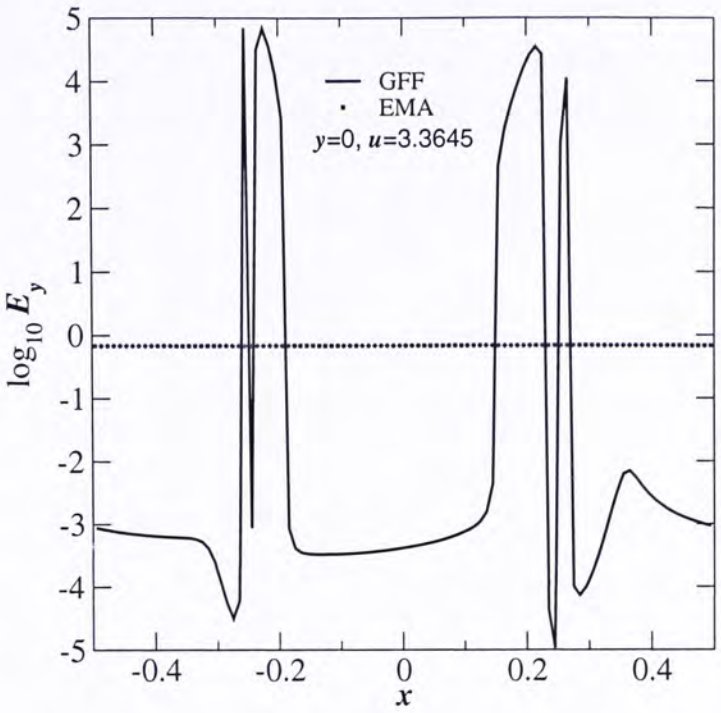

Figure 3.5: $\log_{10}E_y$ found by GFF (solid line) and $\log_{10}E_y$ found by EMA (dots) plotted against x for $u = 3.3645$ (surface plasmon resonance). There is a great enhancement of electric field and it is clear that EMA cannot predict this enhancement.

3.4 Discussion

It is quite surprising to note that the strengths of electric field at both medium across the interface are quite similar and EMA gives excellent description of the electric field except near a surface plasmon resonance. Here we give a possible explanation. In our study, a constant external field is applied to the interface. As a result, we are dealing with quasi-static limit in which the interface cannot be resolved. In other words, we can distinguish medium 1 or medium 2 far away from the interface unambiguously but we cannot do so inside the interface region. We can regard the interface region as a graded region in which one component varies gradually and continuously to other component, as shown

in figure 3.4 (b). In this way, an effective medium is just suitable to describe the physics inside the interface region [14–17]. This is the reason why EMA gives excellent description of the electric field inside the interface region.

Chapter 4

Application of GFF in cylindrical clusters

The hot field of plasmonic relies on the interactions between electromagnetic fields and metallic nanostructures. The interactions can be very important if resonant response occurs inside the structure and these resonances correspond to the Bergman-Milton electrostatic resonances [23–25, 29, 30]. In this chapter, we would characterize the electrostatic resonance of cylindrical cluster by calculating the pole spectrum using GFF. For two cylindrical particles, the results are in excellent agreement with the exact results from the multiple image method [45, 48] and normal-mode expansion method [38]. Our results also show in good agreement with three cylindrical particles arranging in an equilateral triangle [41].

4.1 Review of Bergman's spectral representation

In this section, Bergman's spectral representation would be re-iterated [23–25]. We consider a two-component composite in which inclusions of dielectric constant ϵ_1 are embedded in a homogeneous medium of dielectric constant ϵ_2. We will restrict our discussion to a quasi-static approximation (or long

wavelength approximation). In this approximation, the whole composite can be regarded as an effective homogeneous one with effective linear dielectric constant defined as

$$\epsilon_e = \frac{1}{V}\int \epsilon(\mathbf{r})\frac{\mathbf{E}_0 \cdot \mathbf{E}}{E_0^2} dV, \tag{4.1}$$

where $\mathbf{E}_0$ is the applied electric field along y direction and $\mathbf{E}$ is the local electric field. It should be noted that $\mathbf{E}$ is curl free under long wavelength approximation. As a result, it can be obtained from $\mathbf{E} = -\nabla\phi$. The dielectric function $\epsilon(\mathbf{r})$ is given by

$$\epsilon(\mathbf{r}) = \epsilon_2\left(1 - \frac{1}{s}\theta(\mathbf{r})\right) \tag{4.2}$$

and $\theta(\mathbf{r})$ is a characteristic function which equals 1 if $\mathbf{r} \in V_1$ and 0 otherwise. Note that $s = (1 - \epsilon_1/\epsilon_2)^{-1}$ is the material parameter which is independent to the geometry of the composite. The potential of the whole space satisfies Laplace's equation

$$\nabla \cdot [\epsilon(\mathbf{r})\nabla\phi(\mathbf{r})] = 0 \tag{4.3}$$

subject to the applied field $\mathbf{E_0} = -\mathbf{E_0}\hat{\mathbf{y}}$. Taking advantage of Green's theorem, we are able to transform Eq.(4.3) to

$$\phi(\mathbf{r}) = -E_0 y + \frac{1}{s}\int dV'\theta(\mathbf{r}')\nabla' G(\mathbf{r},\mathbf{r}') \cdot \nabla'\phi(\mathbf{r}'), \tag{4.4}$$

where $G(\mathbf{r},\mathbf{r}') = 1/4\pi\,|\mathbf{r} - \mathbf{r}'|$. Bergman uses this equation to define an volume integral-differential Hermitian operator

$$\hat{\Gamma} = \int dV'\theta(\mathbf{r}')\nabla' G(\mathbf{r},\mathbf{r}') \cdot \nabla', \tag{4.5}$$

and inner product

$$\langle\phi|\psi\rangle = \int dV\theta(\mathbf{r})\nabla\phi^* \cdot \nabla\psi. \tag{4.6}$$

It should be noted that $\langle\phi|\psi\rangle$ and $\langle\psi|\phi\rangle$ are complex conjugate under this definition. Equation (4.4) can be written as

$$\phi(\mathbf{r}) = -E_0 y + \frac{1}{s}\hat{\Gamma}\phi(\mathbf{r}). \tag{4.7}$$

The eigenvalues problem of $\hat{\Gamma}$ reads

$$\hat{\Gamma}\,|\phi_n\rangle = s_n\,|\phi_n\rangle\,. \tag{4.8}$$

As a result, the potential can be expanded in series of eigenfunctions. From equation (4.7), ϕ exists a symbolic solution

$$|\phi\rangle = \frac{-E_0 s}{s-\hat{\Gamma}}\,|y\rangle\,. \tag{4.9}$$

By inserting an identity operator

$$\hat{I} = \sum_n \frac{|\phi_n\rangle\,\langle\phi_n|}{\langle\phi_n|\phi_n\rangle}, \tag{4.10}$$

the potential ϕ can be expressed in a series of eigenfunctions

$$\begin{aligned} |\phi\rangle &= \frac{-E_0 s}{s-\hat{\Gamma}}\left(\sum_n \frac{|\phi_n\rangle\,\langle\phi_n|}{\langle\phi_n|\phi_n\rangle}\right)|y\rangle\,, \\ &= \sum_n \left(\frac{-E_0 s}{s-s_n}\right)\frac{|\phi_n\rangle\langle\phi_n|y\rangle}{\langle\phi_n|\phi_n\rangle}. \end{aligned} \tag{4.11}$$

The effective dielectric constant can be expressed analytically

$$\begin{aligned} \frac{\epsilon_e}{\epsilon_2} &= \frac{1}{\epsilon_2 V E_0}\int \epsilon_2\left(1-\frac{1}{s}\,\theta(\mathbf{r})\right)\hat{y}\cdot\mathbf{E}dV, \\ &= \frac{1}{VE_0}\int dV E_y - \frac{1}{sVE_0}\int dV\theta(\mathbf{r})\,(\nabla y\cdot\nabla\phi)\,, \\ &= 1+\frac{1}{sVE_0}\langle y|\phi\rangle. \end{aligned} \tag{4.12}$$

Bergman further introduces the reduced response

$$F(s) = 1-\frac{\epsilon_e}{\epsilon_2}, \tag{4.13}$$

and substitutes equation (4.11) into equation (4.12), he find

$$F(s) = \frac{1}{V}\sum_n \frac{|\langle y|\phi_n\rangle|^2}{\langle\phi_n|\phi_n\rangle}\left(\frac{1}{s-s_n}\right). \tag{4.14}$$

The effective dielectric constant can be expressed as

$$\epsilon_e = \epsilon_2\left(1 - \sum_n \frac{f_n}{s-s_n}\right), \tag{4.15}$$

where f_n is given by

$$f_n = \frac{1}{V}\frac{|\langle y|\phi_n\rangle|^2}{\langle\phi_n|\phi_n\rangle}. \tag{4.16}$$

We can obtain the following sum rule of f_n

$$\begin{aligned}\sum_n f_n &= \frac{1}{V}\langle y|y\rangle, \\ &= \frac{1}{V}\int dV\theta(\mathbf{r})\nabla y\cdot\nabla y, \\ &= p_1,\end{aligned} \tag{4.17}$$

where p_1 is the volume fraction of the ϵ_1 component. Moreover, Bergman proposes that if the inclusion is isotropic, there exists another sum rule [49, 50]

$$\sum_n s_n f_n = \frac{1}{2}p_1(1-p_1). \tag{4.18}$$

4.2 Extension of Bergman's spectral representation using Green Function Formalism

Now we are in a position to extend Bergman's spectral representation using GFF. According to GFF, equation (4.4) can be transformed to

$$\left(1 - \frac{1}{s}\theta(\mathbf{r})\right)\phi(\mathbf{r}) = -E_0 y + \frac{1}{s}\oint_S dS'[\hat{\mathbf{n}}'\cdot\nabla' G(\mathbf{r},\mathbf{r}')]\phi(\mathbf{r}), \tag{4.19}$$

where $s = 1/u$. When $\mathbf{r}\in S$, equation (4.19) becomes

$$\phi(\mathbf{r}) = -E_0 y + \frac{1}{s}\oint_S dS'[\hat{\mathbf{n}}'\cdot\nabla' G(\mathbf{r},\mathbf{r}')]\phi(\mathbf{r}). \tag{4.20}$$

With reference to equation (4.20), we are able to convert a volume integral differential operator $\hat{\Gamma}$ to a surface integral-differential non-Hermitian operator $\hat{\Gamma}'$, which satisfies

$$\hat{\Gamma}' \equiv \oint_S dS'[\hat{\mathbf{n}}' \cdot \nabla' G(\mathbf{r}, \mathbf{r}')] \tag{4.21}$$

and the inner product is given by

$$\langle \phi | \psi \rangle = \oint_S dS[\hat{\mathbf{n}} \cdot \nabla \phi] \psi. \tag{4.22}$$

It should be noted that $\langle \phi | \psi \rangle$ does not necessarily identical to $\langle \psi | \phi \rangle$ according to the above definition. As a result, equation (4.20) can be transformed to

$$\phi(\mathbf{r}) = -E_0 y + \frac{1}{s} \hat{\Gamma}' \phi(\mathbf{r}). \tag{4.23}$$

It is the same equation in (4.7). The eigenvalues problem of $\hat{\Gamma}'$ is formulated in the absence of applied field. Note that $\hat{\Gamma}'$ is not necessary Hermitian. From now on, we denote s_n, $|R_n\rangle$ and $\langle L_n|$ are the nth eigenvalue, right eigenvector and left eigenvector of $\hat{\Gamma}'$ respectively. The surface integral operator is easier to handle than volume integral operator. However, we have to pay a price that we need to deal with bi-orthogonal system due to possible non-Hermitian nature of the operator. We would like to stress that the eigenvectors only represents the potential on the surface but not the whole volume. By the use of GFF, it is easy to find the eigenvectors of the whole volume by eigenvectors on the surface.

With the same procedure, the potential can be expanded in series of eigenvectors

$$|\phi\rangle = \sum_n \left(\frac{-E_0 s}{s - s_n} \right) \frac{|R_n\rangle \langle L_n | y \rangle}{\langle L_n | R_n \rangle}. \tag{4.24}$$

The effective dielectric constant ϵ_e can be expressed according to equation (4.1)

$$\begin{aligned}
\frac{\epsilon_e}{\epsilon_2} &= \frac{1}{\epsilon_2 V E_0}\int \epsilon_2\left(1-\frac{1}{s}\,\theta(\mathbf{r})\right)\hat{y}\cdot\mathbf{E}dV, \\
&= \frac{1}{VE_0}\int dV E_y - \frac{1}{sVE_0}\int dV\theta(\mathbf{r})\left(\nabla y\cdot\nabla\phi\right), \\
&= 1+\frac{1}{sVE_0}\oint_S dS[\hat{\mathbf{n}}\cdot\nabla y]\phi, \\
&= 1+\frac{1}{sVE_0}\langle y|\phi\rangle. \qquad (4.25)
\end{aligned}$$

With the same definition of dielectric response, we find

$$F(s)=\frac{1}{V}\sum_n \frac{\langle y|R_n\rangle\langle L_n|y\rangle}{\langle L_n|R_n\rangle}\left(\frac{1}{s-s_n}\right), \qquad (4.26)$$

where f_n is given by

$$f_n=\frac{1}{V}\frac{\langle y|R_n\rangle\langle L_n|y\rangle}{\langle L_n|R_n\rangle}. \qquad (4.27)$$

It should be stressed that $\langle y|R_n\rangle\langle L_n|y\rangle$ does not equal $|\langle y|\phi_n\rangle|^2$. However, the sum rule of f_n still holds

$$\begin{aligned}
\sum_n f_n &= \frac{1}{V}\langle y|y\rangle, \\
&= \frac{1}{V}\oint dS[\hat{\mathbf{n}}\cdot\nabla y]y, \\
&= \frac{1}{V}\int_{V_1} dV\nabla\cdot\vec{y}, \\
&= \frac{V_1}{V}. \qquad (4.28)
\end{aligned}$$

4.3 Finding pole spectrum using Green Function Formalism

With the formalism in the previous section, we are now in a position to find the pole spectrum (s_n and f_n) of some cylindrical clusters. For illustration, we consider the case in which two cylinders embedding in a homogeneous host

medium. The boundary of the first and the second cylinders satisfies $r = f(\theta)$ and $r = g(\theta)$ respectively, as shown in the figure 4.1.

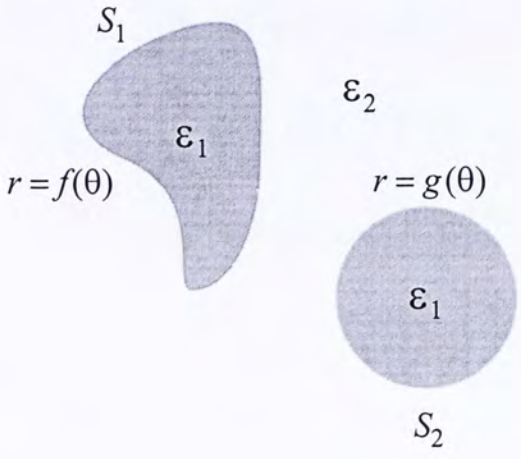

Figure 4.1: Schematic diagram showing two cylinders embedding in a homogeneous host.

By GFF, the potential at the surface of the cylinders satisfies the following integral equation

$$\phi(\mathbf{r}) = -E_0 y + \frac{1}{s}\oint_{S_1} dS'[\hat{\mathbf{n}}' \cdot \nabla' G(\mathbf{r}, \mathbf{r}')]\phi(\mathbf{r}') + \frac{1}{s}\oint_{S_2} dS'[\hat{\mathbf{n}}' \cdot \nabla' G(\mathbf{r}, \mathbf{r}')]\phi(\mathbf{r}'). \tag{4.29}$$

In order to solve the above integral equations, we express the potential at the surface of cylinders by step functions $\psi_j(\theta)$

$$\phi_{S_1}(\theta) = \sum_n P_j \psi_j(\theta), \tag{4.30}$$

$$\phi_{S_2}(\theta) = \sum_n Q_j \psi_j(\theta), \tag{4.31}$$

where

$$\psi_j(\theta) = \begin{cases} 1 & ,\theta_i - \frac{c}{2} < \theta < \theta_i + \frac{c}{2}; \\ 0 & ,\text{otherwise} \end{cases} \tag{4.32}$$

where c is the width of the step function. The following equations can be obtained

$$\sum_n P_j\psi_j(\theta) = -E_0 y + \frac{1}{s}\int_{S_1} d\theta' f(\theta')[\hat{\mathbf{n}}'\cdot\nabla' G_{11}]\sum_n P_j\psi_j(\theta') + \frac{1}{s}\int_{S_2} d\theta' g(\theta')[\hat{\mathbf{n}}'\cdot\nabla' G_{12}]\sum_n Q_j\psi_j(\theta'), \quad (4.33)$$

$$\sum_n Q_j\psi_j(\theta) = -E_0 y + \frac{1}{s}\int_{S_1} d\theta' f(\theta')[\hat{\mathbf{n}}'\cdot\nabla' G_{21}]\sum_n P_j\psi_j(\theta') + \frac{1}{s}\int_{S_2} d\theta' g(\theta')[\hat{\mathbf{n}}'\cdot\nabla' G_{22}]\sum_n Q_j\psi_j(\theta'), \quad (4.34)$$

where

$$G_{11} = G(f(\theta),\theta; f(\theta'),\theta'), \quad (4.35)$$

$$G_{12} = G(f(\theta),\theta; g(\theta'),\theta'), \quad (4.36)$$

$$G_{21} = G(g(\theta),\theta; f(\theta'),\theta'), \quad (4.37)$$

$$G_{22} = G(g(\theta),\theta; g(\theta'),\theta'). \quad (4.38)$$

By integrating both sides by $\int d\theta\psi_i(\theta)$, the following matrix equation can be obtained

$$\begin{pmatrix} P \\ Q \end{pmatrix} = -E_0\mathbf{V} + \frac{1}{s}\begin{pmatrix} M_{11} & M_{12} \\ M_{21} & M_{22} \end{pmatrix}\begin{pmatrix} P \\ Q \end{pmatrix}. \quad (4.39)$$

which is equivalent to

$$s\mathbf{A} = -E_0\mathbf{V} + \mathbf{M}\mathbf{A}, \quad (4.40)$$

where

$$A_i = \begin{cases} P_i, & \text{if } i \le n \\ Q_{i-n}, & \text{if } i > n \end{cases}, \quad (4.41)$$

$$M_{pq,ij} = \int d\theta \int d\theta' \beta(\theta')[\hat{\mathbf{n}}'\cdot\nabla' G_{pq}]\psi_i(\theta)\psi_j(\theta'), \quad (4.42)$$

$$V_i = \int d\theta\psi_i(\theta) y, \quad (4.43)$$

and p and q can be 1 or 2. $\beta(\theta')$ equals $f(\theta')$ when $q = 1$ and equals $g(\theta')$ when $q = 2$. However, the diagonal element of $\mathbf{M}$ cannot be evaluated directly due to the singularity of G when $i = j$. There are two methods to tackle this problem. Firstly, we can split the surface integral into two parts, say S' and S_δ. S' is just the surface excluding the singular point and we can integrate S_δ analytically. In this case, the diagonal element should be equal to 0.5. Secondly, we can calculate the diagonal element by means of a sum rule

$$\sum_j M_{ij} = 0. \tag{4.44}$$

Since the surface integral is broken down into finite element, the later method is more accurate to calculate the diagonal element. It should be remarked that matrix $\mathbf{M}$ is the matrix representation of the $\hat{\Gamma}'$ operator. As a result, the eigenvalues and eigenvectors of $\mathbf{M}$ are equivalent to that of $\hat{\Gamma}'$ operator. Clearly $\mathbf{M}$ is not a symmetric matrix and there exists two sets of eigenvectors. The eigenvalue problem of $\mathbf{M}$ is formulated in the absence of external field

$$\mathbf{M}|R_n\rangle = s_n|R_n\rangle, \tag{4.45}$$

$$\mathbf{M}^{\mathbf{T}}\langle L_n| = s_n\langle L_n|. \tag{4.46}$$

In this case, s_n, $|R_n\rangle$ and $\langle L_n|$ can be determined and hence f_n can be calculated by equation (4.27). In the next section, we are going to present the pole spectra of some cylindrical clusters.

4.4 Numerical Results

4.4.1 Two approaching cylinders

Consider two uncharged cylinders with radii r and dielectric constant ϵ_1 embedded in a homogeneous host medium with perimittivity ϵ_2. They are separated

by center to center distance d and are subject to an external uniform electric field, as shown in figure 4.2. In the transverse (longitudinal) case, the external electric field is perpendicular (parallel) to the center to center direction of the two cylinders.

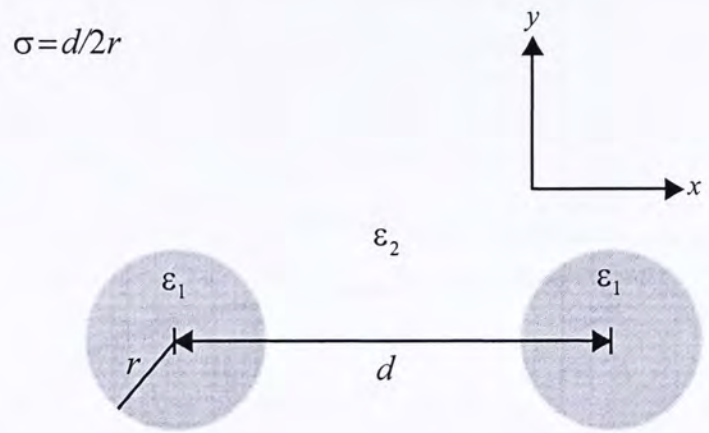

Figure 4.2: Schematic diagram showing two approaching cylinders embedding in a homogeneous host with separation ratio σ.

For two approaching cylinders, the poles and the residues in longitudinal ($f_m^{(L)}$ and $s_m^{(L)}$) and transverse case ($f_m^{(T)}$ and $s_m^{(T)}$) can be solved by multiple image method [48] and their analytical forms are given by

$$f_m^{(L)} = 4me^{-2m\alpha}\sinh^2\alpha, \tag{4.47}$$

$$f_m^{(T)} = 4me^{-2m\alpha}\sinh^2\alpha, \tag{4.48}$$

$$s_m^{(L)} = \frac{1}{2}\left(1-e^{-2m\alpha}\right), \tag{4.49}$$

$$s_m^{(T)} = \frac{1}{2}\left(1+e^{-2m\alpha}\right), \tag{4.50}$$

where $\cosh\alpha = d/2r$ and V is the total volume of the composite. The proof is shown in appendix A. Note that there is no closed analytic form for pole spectra when there are more than two cylinders.

In our numerical computation, 90 steps functions are used. Without loss of generality, r is set to 1. In the discussion below, we present $F_n = Vf_n/\pi$ instead of f_n.

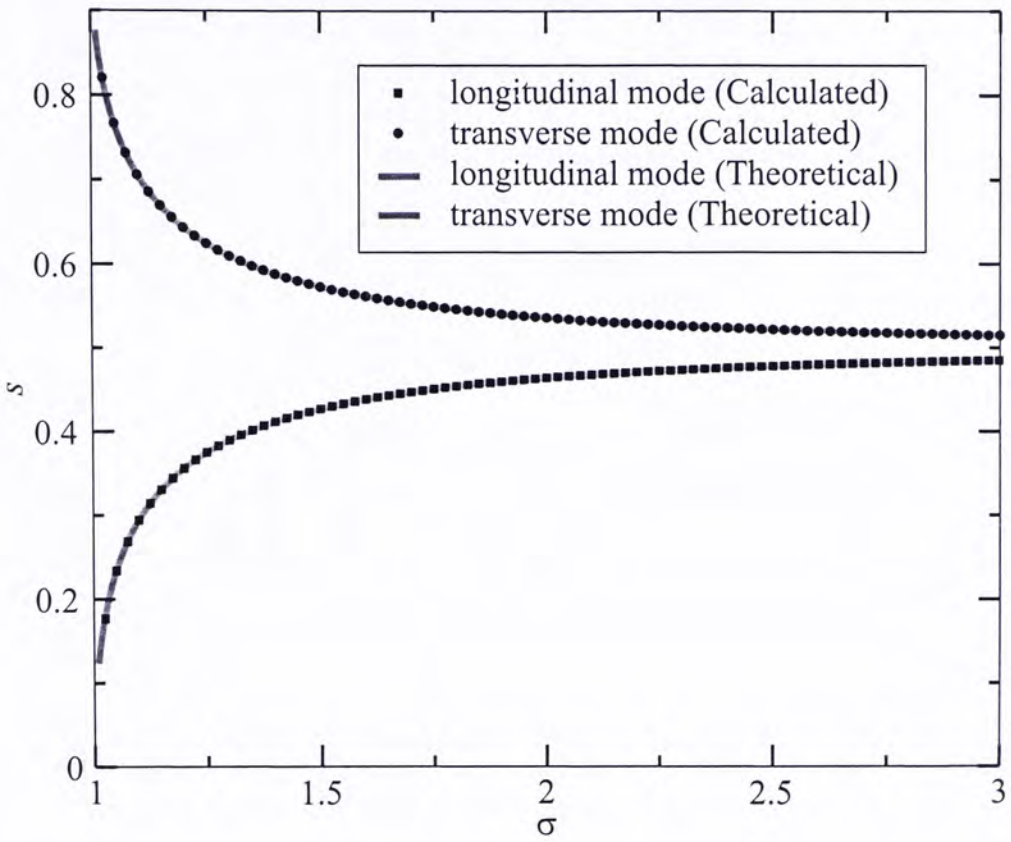

Figure 4.3: Major poles ($s_1^{(L)}$ and $s_1^{(T)}$) against separation ratio $\sigma = d/2r$. Note that the analytic results by equations (4.49) and (4.50) are presented in solid line. The pole calculated by GFF are present as points.

Figure 4.3 shows major poles ($s_1^{(L)}$ and $s_1^{(T)}$) against separation ratio $\sigma = d/2r$. It can be seen that our numerical results match perfectly with the analytic solution. In addition, it is clear that the major poles in transverse mode (given by $s_1^{(T)}$) are always larger than 0.5 while that for longitudinal mode (given by $s_1^{(L)}$) are always larger than 0.5. As shown in the figure, both major poles approach 0.5 when the separation ratio σ increases.

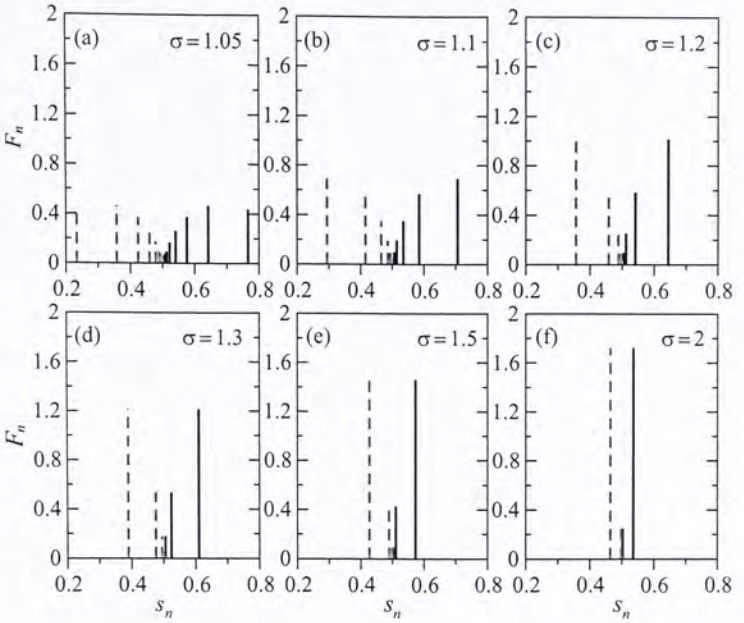

Figure 4.4: Pole spectra of two approaching cylinders with separation ratio: (a) $\sigma = 1.05$; (b) $\sigma = 1.1$; (c) $\sigma = 1.2$; (d) $\sigma = 1.3$; (e) $\sigma = 1.5$; (f) $\sigma = 2$. Note that black solid lines and red dotted lines correspond to the transverse case and longitudinal case respectively.

Figure 4.4 shows the pole spectra of two approaching cylinders with different separation ratio σ. Clearly, only modes larger than 0.5 are excited in transverse case while only modes smaller than 0.5 are excited in longitudinal case. Moreover, the spectra for the longitudinal case are symmetric with that for the transverse case about $s = 0.5$. When two cylinders are closed to one another, the modes are rich. However, modes are concentrated near $s = 0.5$ when two cylinders are far away from one another. It can be explained as follows. For an isolated cylinder, only one pole of 0.5 exists [37, 38]. When two cylinders are far away from one another, it is very similar to isolated cylinder

case.

Here we would like to compare the results with that obtained by Claro *et al.* [38]. Their results are obtained by normal-mode expansion method. Using basis of cylindrical harmonics solutions of Laplace's equation, pole spectra of two approaching cylinders can be found. Figure 4.5 is the Claro's result of the transverse field case with $\sigma = 1.1$. Figure 4.6 shows the same result for the longitudinal field case. Note that the amplitude of mode of Claro's results are two times as our calculated F_n and the reason behind this is the choice of normalization. It is clear that our results show good agreement with Claro's results.

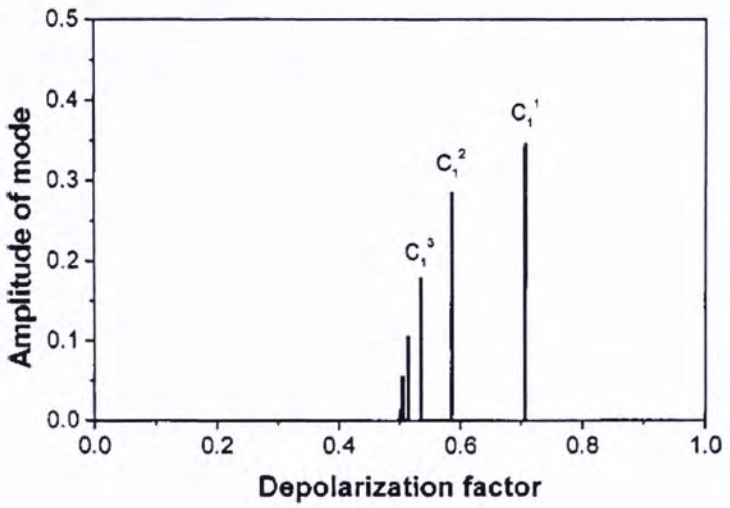

Figure 4.5: A plot of amplitude of mode (same as our $2F_n$) against depolarization factor (same as our s_n) for the transverse field case (Claro *et al.*). It can be seen that only modes with s_n smaller than 0.5 are excited.

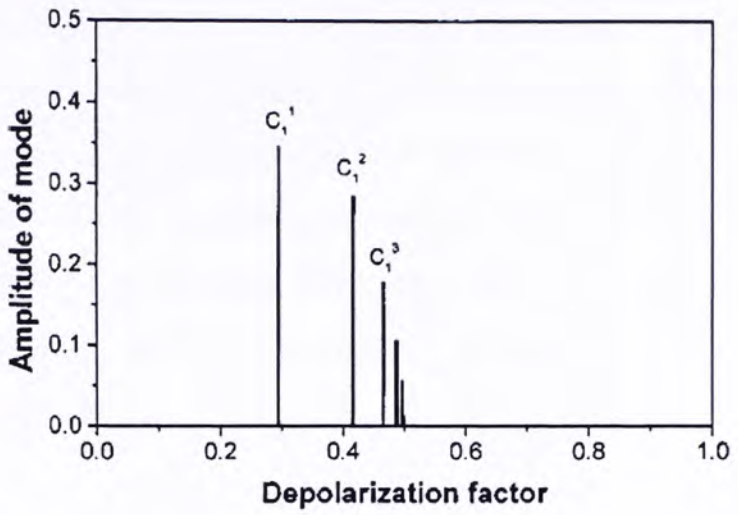

Figure 4.6: A plot of amplitude of mode (same as our $2F_n$) against depolarization factor (same as our s_n) for the longitudinal field case (Claro *et al.*). It can be seen that only modes with s_n larger than 0.5 are excited. The spectrum is a mirror image of that for the transverse field case.

In two cylinders case, the sum rules becomes

$$\sum_n F_n = 2, \tag{4.51}$$

$$\sum_n s_n F_n = 1. \tag{4.52}$$

σ	$\sum_n F_n$ (T)	$\sum_n F_n$ (L)	$\sum_n s_n F_n$ (T)	$\sum_n s_n F_n$(L)	$\sum_n s_n F_n \frac{1}{2}$(T + L)
1.05	2.00000	2.00000	1.22676	0.77326	1.00001
1.10	2.00000	2.00000	1.20661	0.79339	1.00000
1.20	2.00000	2.00000	1.17361	0.82639	1.00000
1.30	2.00000	2.00000	1.14793	0.85207	1.00000
1.50	2.00000	2.00000	1.11111	0.88889	1.00000
2.00	2.00000	2.00000	1.06250	0.93750	1.00000

Table 4.1: The values of sum for two cylinders.

It is instructive to check the sum rules and the calculated sum are shown in table 4.1. In the table, T and L represents transverse and longitudinal case respectively. Our calculated s_n and F_n (either transverse or longitudinal case) matches the first sum rules perfectly. We would like to raise one point here. The second sum rule by Bergman (equation (4.18)) requires inclusion to be isotropic. Clearly, two cylinders array does not satisfy this requirement. In order to match equation (4.52), we need to average the sum from transverse case and longitudinal case.

4.4.2 Three cylinders arranging in a horizontal array

As an extension, it is instructive to consider three uncharged identical cylinders arranging in a horizontal array. The cylinders are separated by separation ratio σ with radii r and dielectric constant ϵ_1. They are subject to an external uniform electric field. The schematic diagram is shown in figure 4.7.

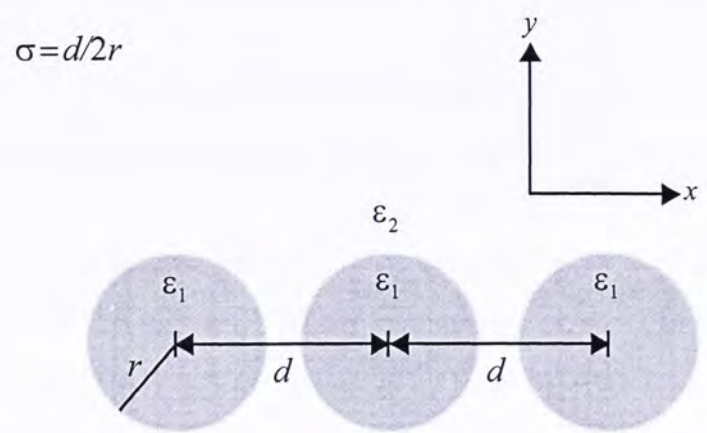

Figure 4.7: Schematic diagram showing three cylinder arranging in a horizontal array with separation ratio σ.

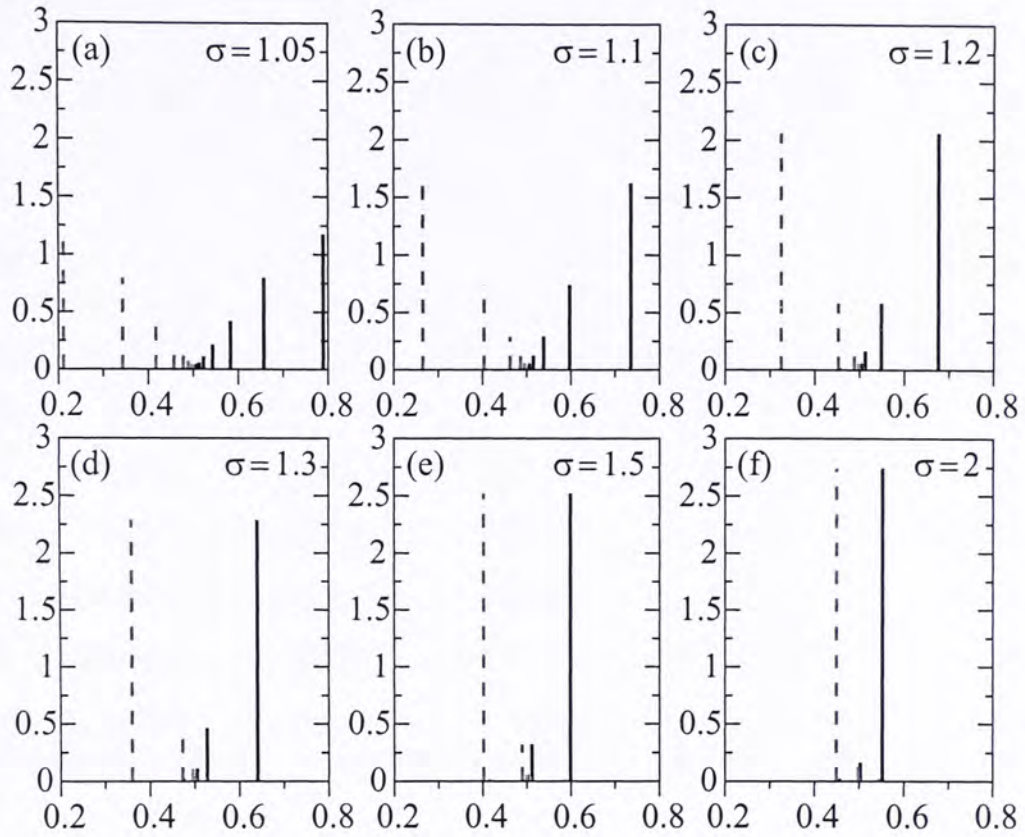

Figure 4.8: Pole spectra of three cylinders arranging in a horizontal array with separation ratio: (a) $\sigma = 1.05$; (b) $\sigma = 1.1$; (c) $\sigma = 1.2$; (d) $\sigma = 1.3$; (e) $\sigma = 1.5$; (f) $\sigma = 2$. Note that black solid lines and red dotted lines correspond to the transverse case and longitudinal case respectively.

The pole spectra are shown in figure 4.8. Similar to two cylinders case, only modes larger than 0.5 are excited in transverse case. On the other hand, only modes smaller than 0.5 are excited in longitudinal case. Moreover, the longitudinal mode spectra is of mirror image to that of the transverse modes. It is also clear that more modes are excited when the cylinders come closer to one another. Comparing with two cylinders case, the pole spectra is spread in a larger extent and more modes are excited.

In the three cylinders case, the sum rules becomes

$$\sum_n F_n = 3, \tag{4.53}$$

$$\sum_n s_n F_n = \frac{3}{2}. \tag{4.54}$$

σ	$\sum_n F_n$ (T)	$\sum_n F_n$ (L)	$\sum_n s_n F_n$ (T)	$\sum_n s_n F_n$(L)	$\sum_n s_n F_n$ $\frac{1}{2}$(T + L)
1.05	3.00000	3.00000	2.01020	0.98972	1.49996
1.10	3.00000	3.00000	1.96488	1.03512	1.50000
1.20	3.00000	3.00000	1.89063	1.10937	1.50000
1.30	3.00000	3.00000	1.83284	1.16716	1.50000
1.50	3.00000	3.00000	1.75000	1.25000	1.50000
2.00	3.00000	3.00000	1.64063	1.35938	1.50000

Table 4.2: The values of sum for three cylinders arranging in a horizontal array.

It is instructive to check the sum rules 4.53 and 4.54. The calculated sum are shown in table 4.2. Our calculated s_n and F_n (either in longitudinal or transverse case) matches sum rule 4.53 perfectly. Similar to previous case, we need to average longitudinal and transverse case in order to match sum rule 4.54.

4.4.3 Three cylinders arranging in an equilateral triangle

In this case, we consider three uncharged identical cylinders with radii r and dielectric constant ϵ_1 embedded in a homogeneous host medium with dielectric constant ϵ_2. They are arranged in an equilateral triangle with separation ratio σ and are subject to an external uniform electric field. The schematic diagram is shown in figure 4.9.

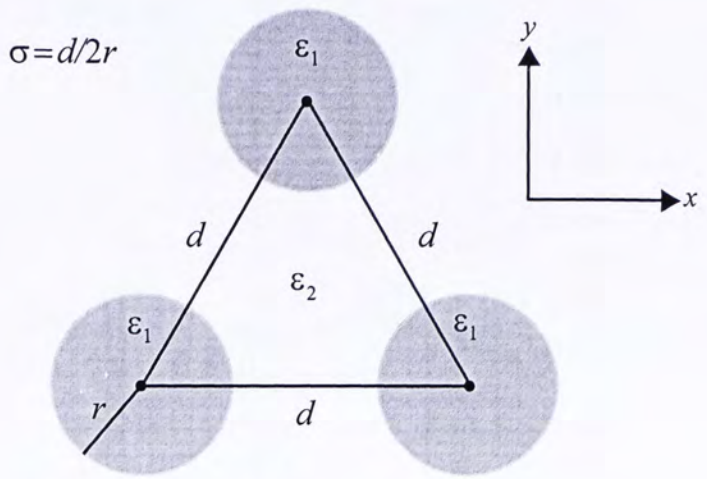

Figure 4.9: Schematic diagram showing three cylinder arranging in an equilateral triangle with separation ratio σ.

The pole spectra are shown in figures 4.10 and 4.11. Note that electric field is applied in y direction and x direction in figure 4.10 and figure 4.11 respectively. As shown in the figures, only a few modes excited when the cylinders are far away from each other. When cylinders come closer and closer, more and more modes are excited. Comparing with previous case, more modes are excited and the modes are spread around $s = 0.5$.

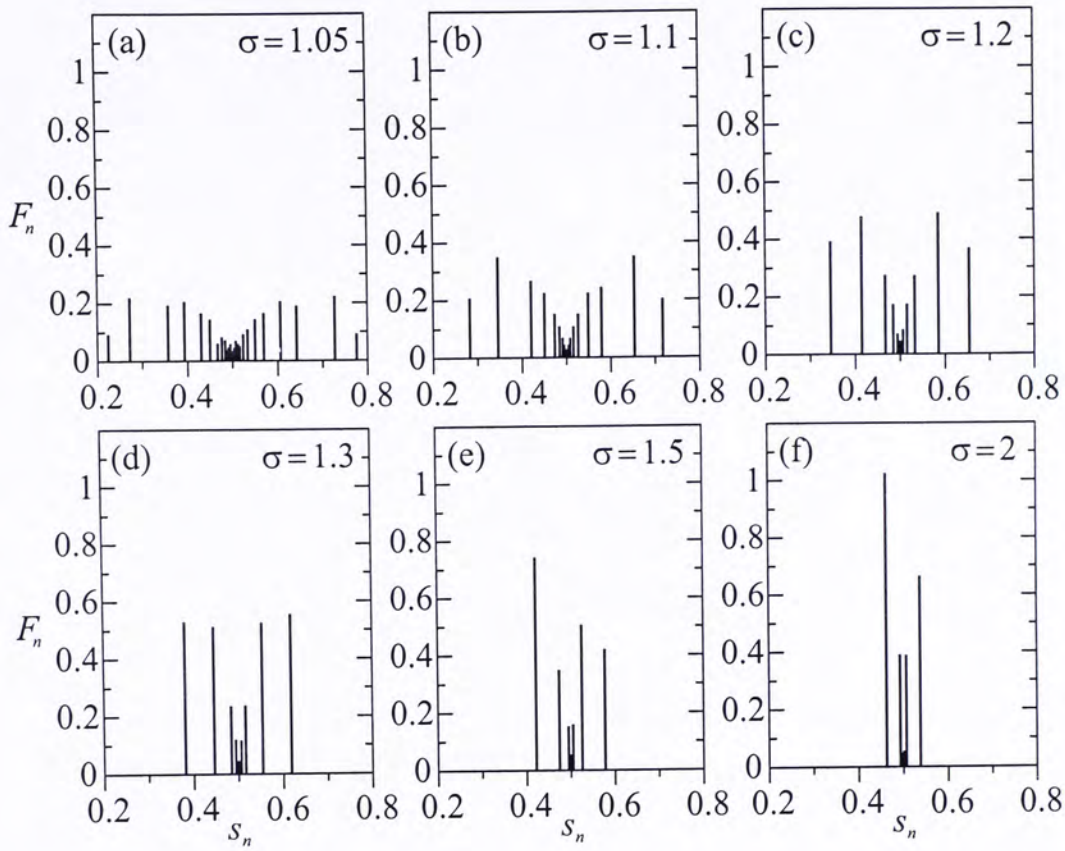

Figure 4.10: Pole spectra of three cylinders arranging in an equilateral triangle with separation ratio: (a) $\sigma = 1.05$; (b) $\sigma = 1.1$; (c) $\sigma = 1.2$; (d) $\sigma = 1.3$; (e) $\sigma = 1.5$; (f) $\sigma = 2$. Note that the external electric field is applied in y direction.

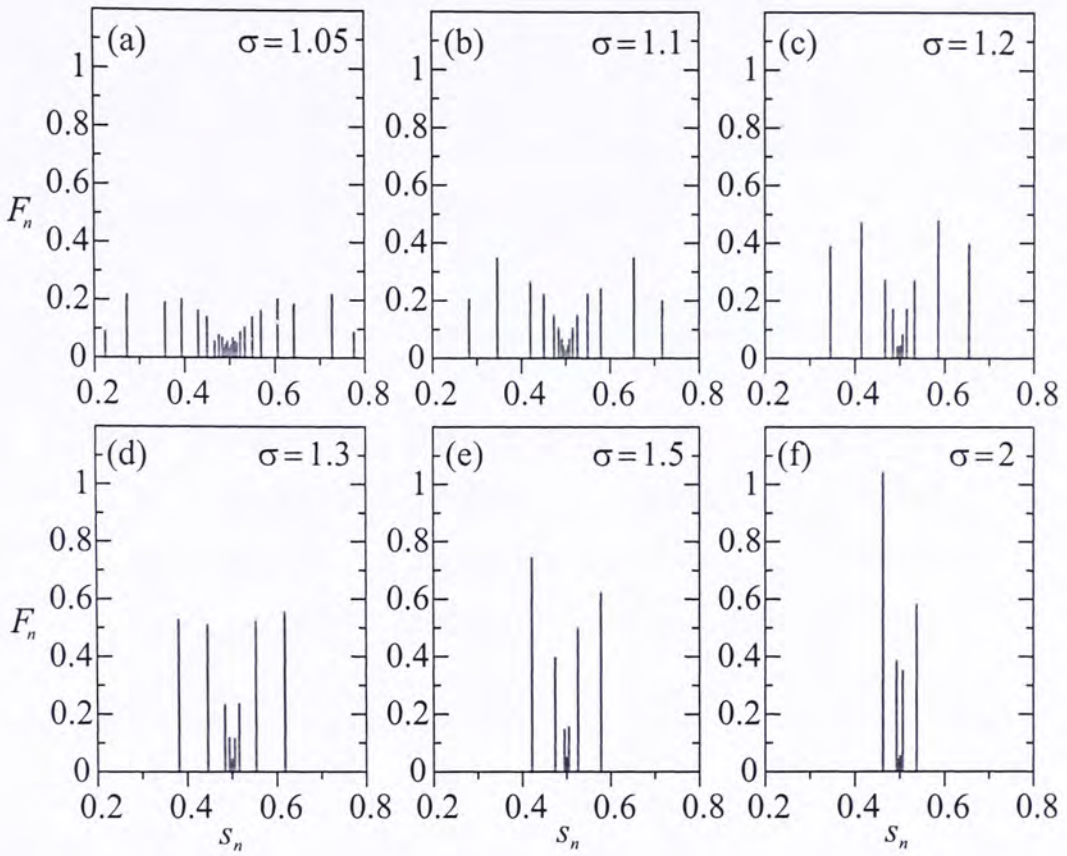

Figure 4.11: Pole spectra of three cylinders arranging in an equilateral triangle with separation ratio: (a) $\sigma = 1.05$; (b) $\sigma = 1.1$; (c) $\sigma = 1.2$; (d) $\sigma = 1.3$; (e) $\sigma = 1.5$; (f) $\sigma = 2$. Note that the external electric field is applied in x direction.

Here we would like to compare the results with McPhedran *et al.* [41]. Using Wijngaard expansion [51] and Rayleigh identity, McPhedran solved Laplace's equation formally with matching of boundary conditions. The eigenstates can be obtained by singular value decomposition method. In McPhedran's set up, three cylinders are arranged in an equilateral triangle with separation ratio $\sigma = 5/3$. They found that one resonance exists when dielectric constant of the cylinders and surrounding medium are -0.653143 and 1 respectively [41]. In our numerical calculation, $s = 0.604909$ is one of the poles when $\sigma = 5/3$. Since

$$\epsilon_1 = 1 - \frac{1}{s}, \tag{4.55}$$

it is clear the dielectric constants of the cylinders should be $1 - 1/0.604909 = -0.653143$, which matches McPhedran's results.

σ	$\sum_n F_n\,(y)$	$\sum_n F_n\,(x)$	$\sum_n s_n F_n\,(x)$	$\sum_n s_n F_n(y)$
1.05	3.00000	3.00000	1.49995	1.49995
1.10	3.00000	3.00000	1.50000	1.50000
1.20	3.00000	3.00000	1.50000	1.50000
1.30	3.00000	3.00000	1.50000	1.50000
1.50	3.00000	3.00000	1.50000	1.50000
2.00	3.00000	3.00000	1.50000	1.50000

Table 4.3: The values of sum rule for three cylinders arranging in equilateral triangle.

It is instructive to check the sum rules 4.53 and 4.54 for this system. The calculated sum are shown in table 4.3. Our calculated s_n and F_n (either x field or y field) matches the sum rules perfectly. The matching of 4.54 is due to the fact that the cylinders are arranging in an isotropic way.

4.4.4 Three cylinders arranging in an isosceles triangle

We consider three uncharged identical cylinders with radii r and dielectric constant ϵ_1 embedded in a homogeneous host medium with dielectric constant ϵ_2. They are arranged in an isosceles triangle with base cylinders separating by a center to center distance d and are subject to an external uniform electric field. Denote the height of the isosceles triangle be H and here we define a height to base ratio $\rho = H/d$. Similar to two cylinders case, we are going to find the pole spectra with different ρ. The schematic diagram is shown in

figure 4.12. In the discussion below, the two base cylinders are separated by a separation ratio $\sigma = 1.1$.

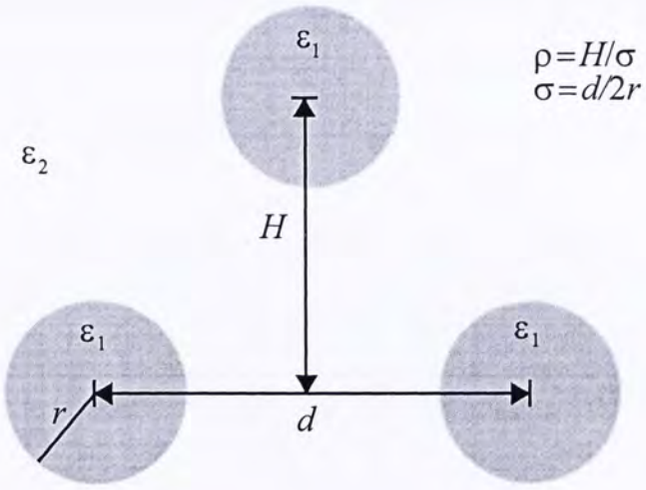

Figure 4.12: Schematic diagram showing three cylinders arranging in an isosceles triangle.

Figures 4.13 and 4.14 shows the pole spectra of three cylinders arranging in an isosceles triangle with different height to base ratio ρ. Note that the electric field is applied in y and x direction in figure 4.13 and 4.14 respectively. As shown in the figures, more modes larger (smaller) than 0.5 are excited when the electric field is applied in y (x) direction. When the upper cylinder is situated near the base cylinders (small value of ρ), modes become richer. When we move the upper cylinder away from the base cylinders, fewer poles are excited. We can also compare the pole spectra in figures 4.13 (d), 4.14 (d) and 4.4 (b). It can be seen that figure 4.13 (d) and 4.14 (d) are similar to that in 4.4 (b), with the enhancement of poles near 0.5. We can understand this as follows. In the case of figures 4.13 (d) and 4.14 (d), the upper cylinder is quite far away from the base cylinders. As a result, there is less interaction between them and we an regard the system as an isolated cylinder (monomer) and two base cylinders (dimer) at a separation $\sigma = 1.1$. Since the pole of isolated cylinder

is located at 0.5, this can explain the enhancement of poles near 0.5 in figures 4.13 (d) and 4.14 (d).

Table 4.4 shows the calculated sum in this case. Our calculated s_n and F_n match the first sum rule perfectly. Since the system is not isotropic, we need to average the sum from transverse and longitudinal case in order to satisfy second sum rule.

ρ	$\sum_n F_n\,(y)$	$\sum_n F_n\,(x)$	$\sum_n s_n F_n\,(y)$	$\sum_n s_n F_n(x)$	$\sum_n s_n F_n\,\frac{1}{2}(x+y)$
1.10	3.00000	3.00000	1.50826	1.49174	1.50000
1.50	3.00000	3.00000	1.57438	1.42562	1.50000
2.00	3.00000	3.00000	1.62082	1.37918	1.50000
5.00	3.00000	3.00000	1.69057	1.30943	1.50000

Table 4.4: The values of sum for three cylinders arranging in an isosceles triangle.

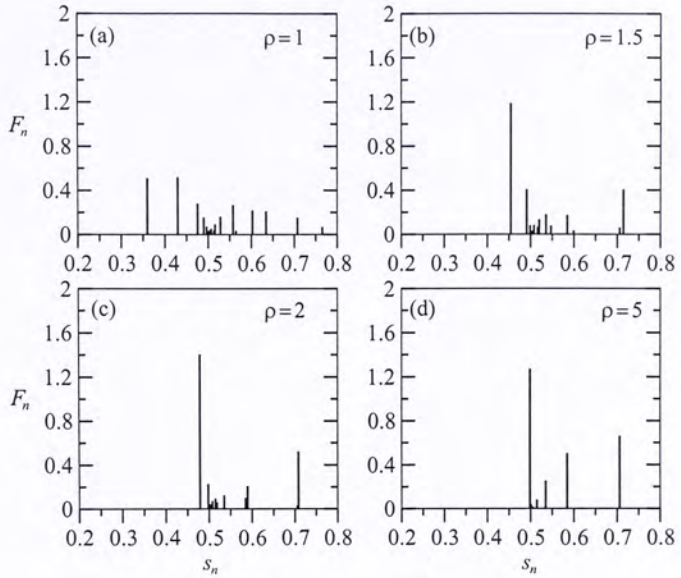

Figure 4.13: Pole spectra of three cylinders arranging in an isosceles triangle with different height to base ratio $\rho = H/d$: (a) $\rho = 1$; (b) $\rho = 1.5$; (c) $\rho = 2$; (d) $\rho = 5$. Note that the electric field is applied in y direction in this case.

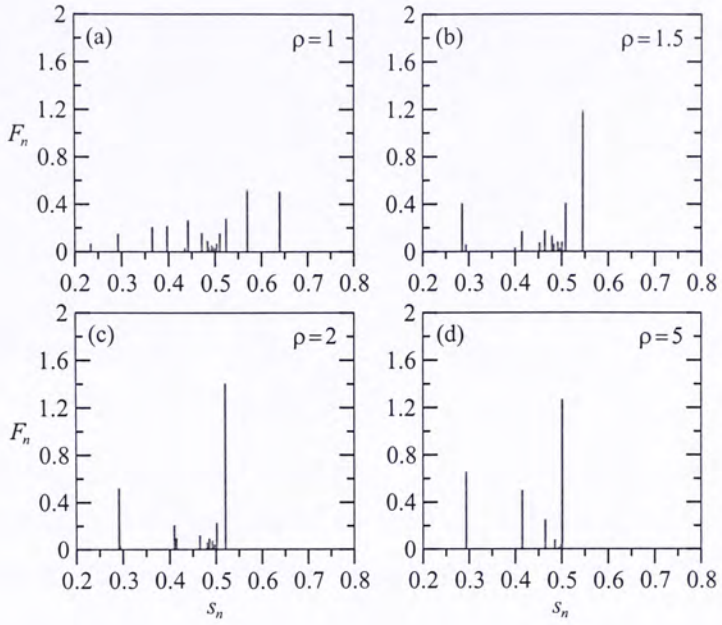

Figure 4.14: Pole spectra of three cylinders arranging in an isosceles triangle with different height to base ratio $\rho = H/d$: (a) $\rho = 1$; (b) $\rho = 1.5$; (c) $\rho = 2$; (d) $\rho = 5$. Note that the electric field is applied in x direction in this case.

Chapter 5

Summary

The thesis mainly concerned about Green function formalism (GFF) which is used compute the local field distribution for an arbitrary interface separating two media of different dielectric constants without matching of complicated boundary conditions.

In the first part of the thesis, we have extended the established GFF to compute the electric field inside the interface region by taking advantage of a sum rule. To our surprise, the strengths of electric fields in both media across the interface are quite similar despite of the large difference in dielectric constants. Moreover, we show that the EMA indeed gives an excellent description of these fields except near a surface plasmon resonance. This provides a great insight that corrugated interfaces can be described by graded interfaces. More work can be done in this direction.

The second part of the thesis concerned about Bergman-Milton electrostatic resonances. Using GFF, we developed an efficient method for the study of spectral representation of two electromagnetic media separated by arbitrary interface based on the GFF, and applied it to the case of cylinder dimers and trimers. We compared the numerical solution of the spectral functions (poles and residues) with the calculations made by using mode expansion technique and multiple image method in the dimer case. The excellent agreement between them indicates that the theoretical formulation is correct and much

more valuable. The case of trimer arranging in an isosceles triangle was analyzed in detail and compared to the dimer case, in an attempt to explore the particle-pair interaction. This complemented previous overwhelming discussions on particle-particle interactions (i.e., dimerization effect). Further theoretical work will be aimed at the localization and delocalization behavior in clusters with increased number of cylinders, and also at the generalization of this approach to three dimensional spheres.

Bibliography

[1] J. D. Jackson, *Classical Electrodynamics*, John Wiley and Sons, US, 1975.

[2] G. Binnig, H. Rohrer, C. Gerber, and E. Weibel, Phys. Rev. Lett. **49**, 57 (1982).

[3] J. Hu, X. D. Xiao, D. F. Ogeletree, and M. Salmeron, Science **268**, 267 (1995).

[4] Z. Y. Li, B. Y. Gu, and G. Z. Yang, Phys. Rev. B **57**, 9225 (1998).

[5] U. Hofer and *et. al.*, Science **277**, 1480 (1997).

[6] K. W. Yu, H. Sun, and J. T. K. Wan, Phys. Rev. B **279**, 78 (2000).

[7] K. W. Yu and J. T. K. Wan, Comput. Phys. Commun. **142**, 368 (2001).

[8] J. Korringa, Physica **13**, 392 (1947).

[9] W. Kohn and N. Rostoker, Phys. Rev. **94**, 1111 (1954).

[10] Y. Gu, K. W. Yu, and H. Sun, Phys. Rev. B **59**, 12847 (1999).

[11] Y. Gu and K. W. Yu, Chinese Physics **11**, 606 (2001).

[12] Y. Gu and Q. H. Gong, J. Phys: Condens. Matter **14**, 6567 (2002).

[13] H. F. Tam, *Local field distribution near corrugated interfaces*, Master's thesis, The Chinese University of Hong Kong, Physics Department, 2003.

[14] C. W. Choy, J. J. Xiao, and K. W. Yu, Physica B **394**, 325 (2007).

[15] J. P. Huang and K. W. Yu, Phys. Rep. **431**, 87 (2006).

[16] B. Xu, J. P. Huang, and K. W. Yu, Phys. Lett. A **357**, 475 (2006).

[17] C. T. Yam, *Dielectric Behavior of Colloidal Suspensions*, Master's thesis, The Chinese University of Hong Kong, Physics Department, 2005.

[18] G. Shvets and Y. A. Urzhumov, Phys. Rev. Lett. **93**, 243902 (2003).

[19] D. R. Fredkin and I. D. Mayergoyz, Phys. Rev. Lett. **91**, 253902 (2003).

[20] P. Robles, F. Claro, and R. Rojas, Phys. Rev. B **71**, 195407 (2005).

[21] I. D. Mayergoyz and Z. Y. Zhang, J. Comp. Elec. **4**, 139 (2005).

[22] I. D. Mayergoyz, D. R. Fredkin, and Z. Y. Zhang, Phys. Rev. B **72**, 155412 (2005).

[23] D. J. Bergman and D. Stroud, Solid State Physics **46**, 147 (1992).

[24] D. J. Bergman, Phys. Rep. **43**, 377 (1978).

[25] D. J. Bergman, Phys. Rev. B **19**, 2359 (1979).

[26] M. I. Stockman, S. V. Faleev, and D. J. Bergman, Phys. Rev. Lett. **87**, 167401 (2001).

[27] W. L. Barnes, A. Dereux, and T. W. Ebbesen, Nature **424**, 824 (2003).

[28] J. J. Xiao, K. Yakubo, and K. W. Yu, Appl. Phys. Lett. **88**, 241111 (2006).

[29] G. W. Milton, J. Appl. Phys. **52**, 5286 (1980).

[30] R. C. McPhedran and G. W. Milton, Appl. Phys. A: Solids Surf. **26**, 207 (1981).

[31] G. W. Milton, *The Theory of Composites*, Cambridge University Press, New York, 2002.

[32] K. Kim, D. Stroud, X. Li, and D. J. Bergman, Phys. Rev. E **71**, 031503 (2005).

[33] J. P. Huang, K. W. Yu, and G. Q. Gu, Phys. Rev. E **65**, 021401 (2002).

[34] J. P. Huang, M. Karttunen, K. W. Yu, and L. Dong, Phys. Rev. E **67**, 021403 (2003).

[35] Y. Gu and Q. Gong, Phys. Rev. B **67**, 014209 (2003).

[36] L. Dong, M. Karttunen, and K. W. Yu, Phys. Rev. E **72**, 016613 (2005).

[37] J. P. Huang, K. W. Yu, and G. Q. Gu, Phys. Rev. E **65**, 021401 (2002).

[38] P. Robles, R. Rojas, and F. Claro, Phys. Rev. E **65**, 036612 (2002).

[39] J. Lei, J. T. K. Wan, K. W. Yu, and H. Sun, Phys. Rev. E **64**, 012903 (2000).

[40] J. J. Xiao, J. P. Huang, and K. W. Yu, Phys. Rev. B **71**, 045404 (2005).

[41] L. Field, N. A. Nicorovici, and R. C. McPhedran, Physica B **394**, 193 (2007).

[42] R. C. McPhedran and G. W. Milton, Proc. R. Soc. Lond. A **411**, 313 (1987).

[43] R. C. McPhedran, Proc. R. Soc. Lond. A **408**, 31 (1986).

[44] R. C. McPhedran, L. Poladian, and G. W. Milton, Proc. R. Soc. Lond. A **415**, 185 (1988).

[45] K. W. Yu and J. T. K. Wan, Comput. Phys. Commun. **129**, 177 (2000).

[46] M. Y. Ng and W. C. Liu, Opt. Express **14**, 4504 (2006).

[47] I. S. Gradshteyn and I. M. Ryzhik, *Table of Integrals, Series and Products*, Academic Press, New York, 1980.

[48] J. P. Huang, *Physics of Colloidal Suspensions*, PhD thesis, The Chinese University of Hong Kong, Physics Department, 2003.

[49] D. J. Bergman, J. Phys. C **12**, 4974 (1979).

[50] D. J. Bergman, *Les Methodes de l'Homogeneisation: Theorie et Applications en Physique*, Edition Evrolles, Paris, 1985.

[51] W. Wijngaard, J. Opt. Soc. Am. **63**, 944 (1973).

[52] B. R. Djordjevic, J. H. Hetherington, and M. F. Thorpe, Phys. Rev. B **53**, 14862 (1996).

[53] J. P. Huang and K. W. Yu, J. Phys.: Condens. Matter **14**, 1213 (2002).

Appendix A

Multiple image method to a pair of cylinders

A.1 Dipole factor of a pair of cylinders

Here we would like to review the multiple image method to a pair of identical cylinders. [45, 48]. We first consider an isolated cylinder with radius r and dielectric constant ϵ_1 embedded in a host with dielectric constant ϵ_2. A dipole moment p will be induced on the isolated cylinder when an external uniform electric field E_0 is applied,

$$p = 2\pi\beta \left(\frac{r}{2}\right)^2 E_0, \tag{A.1}$$

where $\beta = (\epsilon_1 - \epsilon_2)/(\epsilon_1 + \epsilon_2)$ is the dipole factor of an isolated cylinder.

Now, we consider two cylinders with dielectric constant ϵ_1 embedded in host with dielectric constant ϵ_2. They are separated by a center to center distance d and they are subject to external uniform electric field. Similar to the isolated cylinder case, this electric field would induce a dipole moment on each cylinders. Denote the dipole moments of cylinders 1 and 2 as p_{10} and p_{20} respectively. Taking account of image effects, the dipole moment p_{10} induces an image dipole p_{11} on cylinder 2. This dipole moment p_{11} will induces other image dipole on cylinder 1. The same process repeats for p_{20}. As a result,

multiple images are formed and we can obtain two infinite series of the image dipoles for each cylinders and hence the dipole factors of a pair of touching cylinders can be obtained. For two identical cylinders, the total longitudinal and transverse dipole factors (β_L and β_T) are [52]

$$\beta_L = 2\sum_{n=1}^{\infty} \beta^n \left(\frac{\sinh\alpha}{\sinh n\alpha}\right)^2, \tag{A.2}$$

$$\beta_T = 2\sum_{n=1}^{\infty} (-1)^{n+1}\beta^n \left(\frac{\sinh\alpha}{\sinh n\alpha}\right)^2, \tag{A.3}$$

where $\cos\alpha = d/2r$ and r is the radius of both cylinders.

A.2 Spectral representation

Now, we would like to express the above exact dipole factors (A.2) and (A.3) in the spectral representation

$$\beta_L = \sum_{n=1}^{\infty} \frac{F_m^{(L)}}{s - s_m^L}, \tag{A.4}$$

$$\beta_T = \sum_{n=1}^{\infty} \frac{F_m^{(T)}}{s - s_m^T}, \tag{A.5}$$

where s is a material parameter defined by $s = (1-\epsilon_1/\epsilon_2)$. The above representation has the advantage that the material parameters (such as permittivity and conductivity) are separated from geometric parameters (such as size of particles and geometric arrangement of particles). As a result, the geometric properties are separated from the material parameters during the calculation of the effective dielectric properties of the mixture. In order to express the dipole factors, we need to make use of the following identity for sinh

$$\frac{1}{\sinh^2 nx} = \sum_{m=1}^{\infty} 4me^{-2mnx}. \tag{A.6}$$

Hence, the longitudinal dipole factor can be expressed as

$$\begin{aligned}
\beta_L &= 2\sinh^2\alpha \sum_{n=1}^{\infty} b^n \sum_{m=1}^{\infty} 4me^{-2mn\alpha}, \\
&= 8\sinh^2\alpha \sum_{m=1}^{\infty} m \sum_{n=1}^{\infty} b^n e^{-2mn\alpha}, \\
&= \sum_{m=1}^{\infty} \frac{4me^{-2m\alpha}\sinh^2\alpha}{s - \frac{1}{2}\left(1 - e^{-2m\alpha}\right)}. \qquad \text{(A.7)}
\end{aligned}$$

Note that we have expressed $b = 1/(1-2s)$ in the last step. The derivation of transverse case can be obtained similarly. Finally, the residues ($F_m^{(L)}$ and $F_m^{(T)}$) and the poles ($s_m^{(L)}$ and $s_m^{(T)}$) are explicitly given by

$$f_m^{(L)} = 4me^{-2m\alpha}\sinh^2\alpha, \qquad \text{(A.8)}$$

$$f_m^{(T)} = 4me^{-2m\alpha}\sinh^2\alpha, \qquad \text{(A.9)}$$

$$s_m^{(L)} = \frac{1}{2}\left(1 - e^{-2m\alpha}\right), \qquad \text{(A.10)}$$

$$s_m^{(T)} = \frac{1}{2}\left(1 + e^{-2m\alpha}\right). \qquad \text{(A.11)}$$

Appendix B

Illustration of Bergman-Milton Spectral Representation

Here we would like to illustrate Berman-Milton Sepctral represenation in a clear way [15]. In Bergman-Milton Spectral Representation, the crucial step is to define a material parameter

$$s = \left(1 - \frac{\epsilon_1}{\epsilon_2}\right)^{-1} \tag{B.1}$$

and hence the reduced response

$$F(s) = 1 - \frac{\epsilon_1}{\epsilon_2} \tag{B.2}$$

can be rewritten as

$$F(s) = \sum_n \frac{F_n}{s - s_n}. \tag{B.3}$$

In the above representation, F_n and s_n are the n-th microstructure parameters of the composite materials [24]. The range of s_n is from zero to one and s_n and F_n satisfied two sum rules

$$\sum_n f_n = p_1, \tag{B.4}$$

$$\sum_n s_n f_n = \frac{1}{2} p_1 (1 - p_1). \tag{B.5}$$

Below we would like to illustrate the spectral reprsentation by the capacitance of simple geometry [53] and a parallel plate capacitor is considered as an example. Two cases will be discussed including the series combination and the parallel combination.

B.1 Series combination

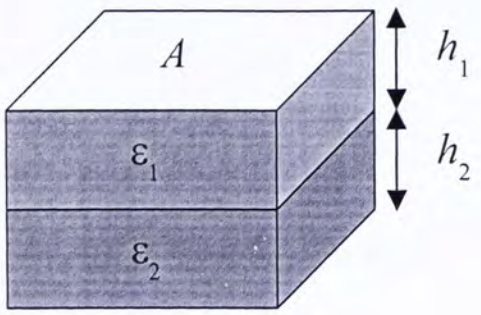

Figure B.1: Schematic diagram showing two dielectric slabs connecting in series combination.

As shown in above diagram, one dielectric slab of dielectric constant ϵ_1 and thickness h_1 and one dielectric slab of dielectric constant ϵ_2 of thickness h_2 are inserted into a parallel-plate capacitor of total thickness h. Both dielectric slabs have the same area A. As a result, the overall capacitance C is given by

$$C = \left(C_1^{-1} + C_2^{-1}\right)^{-1}, \tag{B.6}$$

where $C_1 = \epsilon_1 A/h_1$ and $C_2 = \epsilon_2 A/h_2$. We may also regard the composite dielectric as a homogeneous dielectric of dielectric constant ϵ_e and hence the overall capacitance C is given by

$$C = \frac{\epsilon_e A}{h}. \tag{B.7}$$

Since $\epsilon_1 = \epsilon_2(1 - 1/s)$, we can express C in terms of s

$$C = \frac{A\epsilon_2}{h} - \frac{A\epsilon_2 h_1/h^2}{s - h_2/h}. \tag{B.8}$$

It is instructive to rewrite equation B.2 in terms of capacitance

$$F(s) = 1 - \frac{C}{C_0}, \tag{B.9}$$

where $C_0 = \epsilon_2 A/h$ is the capacitance when the plates are all filled with dielectric material of ϵ_2. As a result, we obtain

$$F(s) = \frac{h_1/h}{s - h_2/h}. \tag{B.10}$$

Comparing B.10 with B.2, we can obtain F_1 and s_1

$$F_1 = \frac{h_1}{h}, \tag{B.11}$$

$$s_1 = \frac{h_2}{h}. \tag{B.12}$$

Note that F_1 obtained equals the volume fraction of dielectric of ϵ_1 and s_1 must be ranged from zero to one.

B.2 Parallel combination

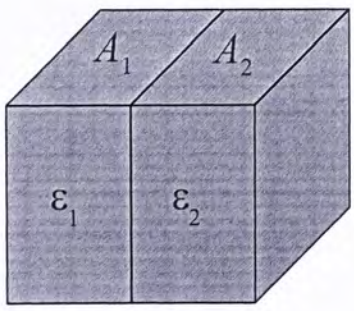

Figure B.2: Schematic diagram showing two dielectric slabs connecting in parallel combination.

Now we would like to consider the parallel combination in which a dielectic slab with dielectric constant ϵ_1 and area A_1 and a dielectric slab with dielectric constant ϵ_2 and area A_2 are inserted into a parallel plate capacitor. The total area is then given by $A = A_1 + A_2$. The overall capacitance is given by

$$C = C_1 + C_2, \tag{B.13}$$

where $C_1 = \epsilon_1 A_1/h$ and $C_2 = \epsilon_2 A_2/h$. Similar to previous case, C can also be given by $C = \epsilon_e A/h$. After spectral represenation, the equivalent capacitance is given by

$$C = \frac{\epsilon_2 A}{h} - \frac{\epsilon_2 A_1}{hs}. \tag{B.14}$$

Similar to previous case, we can write $F(s) = 1 - C/C_0$. Thus, we obtain

$$F(s) = \frac{A_1/A}{s}. \tag{B.15}$$

Comparing this equation with B.2, we can obtain F_1 and s_1

$$F_1 = \frac{A_1}{A}, \tag{B.16}$$

$$s_1 = 0. \tag{B.17}$$

Since $A_1/A = p_1$, F_1 obtained is the volume fraction of dielectric ϵ_1.